Stream thermal regimes within an alpine discontinuous permafrost catchment, southern Yukon Territory

Stream thermal regimes within an alpine discontinuous permafrost catchment, southern Yukon Territory

By: Ryan L. Rolick, B.Sc., GIT

A Thesis Submitted to the School of Graduate Studies in Partial Fulfillment of the Requirements for the Degree Master of Science

McMaster University

MASTER OF SCIENCE (2017) MCMASTER UNIVERSITY
(EARTH AND ENVIRONMENTAL SCIENCE) HAMILTON, ONTARIO

TITLE: Stream thermal regimes within an alpine discontinuous permafrost catchment, southern Yukon Territory

AUTHOR: Ryan L. Rolick, B.Sc., GIT – Physical Geography (Simon Fraser University)

SUPERVISOR: Dr. Sean K. Carey

NUMBER OF PAGES: ix, 69

Abstract

Stream temperature, which influences many biogeochemical processes, is controlled by the exchange of water and energy across the stream surface, banks, and bed. A stream's thermal sensitivity is its sensitivity to changes in air temperature and is increasingly important with projected warming in northern regions. As the thermal dynamics in permafrost underlain headwater streams are poorly documented, this study examines the thermal signals of two neighboring alpine streams (Granger Creek, GC and Buckbrush Creek, BB) within the Wolf Creek Research Basin (WCRB), Yukon Territory, and quantifies the dominant energy fluxes through an energy budget approach. A 1950 m study reach was established in each stream where water temperature, vertical streambed temperature, and stream discharge were measured. Distinct thermal heterogeneity is observed in each stream, with areas of persistent temperature decrease along their lengths, minimal downstream increase in stream temperature in GC, and an overall decrease in downstream temperature in BB. These observations are indicative of focused groundwater upwelling, low thermal sensitivity, and an increasing downstream influence of groundwater. This is inferred from increases in specific conductivity (2 µS/cm – 20 µS/cm) at locations of temperature decrease, and patterns in low (high) mean air-water linear regression slope (intercept) values. With distance downstream, regression slope (intercept) in GC went from 0.37 (1.2˚C) upstream to 0.33 (2.6˚C) at the outlet. Similarly, in BB regression slope (intercept) went from 0.37 (2.1˚C) upstream to 0.24 (3.3˚C) downstream. These patterns also indicate an overall lower thermal sensitivity and greater groundwater influence across the study reach of BB. Downwelling is observed at locations of vertical temperature profiles in each stream through efficient downward propagation of the diel temperature signal into the streambed, indicating hyporheic exchange. The energy balance indicates a large unaccounted for sink in BB, further denoting a larger groundwater influence in its study reach. These findings highlight the importance for continued study of thermal regimes and the complicated interconnections between heat exchange processes in alpine catchments in permafrost regions.

Acknowledgements

First and foremost, I would like to thank my supervisor Dr. Sean Carey for taking me on as a student, giving me the opportunity to choose a project that was outside of his area of expertise, and being an excellent mentor along the way. He is always able to offer a new perspective and knows when to crack a joke at the perfect time to help lighten the mood. Sean has given me likely one of the best student-supervisor experiences I could have had and has well prepared me to continue onwards into the field of hydrology.

Thank you to Dr. Barret Kurylyk, for being extremely knowledgeable in the field of stream thermal regimes, offering rapid feedback, and being an all-around great guy. I was able to get this far due to his insightful suggestions and unending patience. Thanks to Dr. Gordon Drewitt for his MATLAB wizardry, I have learned so much from him this past year. Dr. Jim Smith is also thanked for helping me to understand the intricacies of contaminant hydrogeology with some laughs along the way.

Thanks to my student colleagues in the Watershed Hydrology Group:
Victor Tang for his help with MATLAB and being a formidable opponent in the squash court.
Kelly Biagi for her help with MATLAB, encouragement, and being a great friend.
Supriya Singh for being a wonderful labmate, classmate, and friend.

A special thanks to Renée Lemmond for being the best, fittest, funniest, research assistant, ally, sounding board, and friend during a very demanding field season. Thanks to Ric Janowicz for always providing good company, food, and beer during our days-off in Whitehorse.

Thank you to all the wonderful colleagues and teammates that I have had the joy of making in the McMaster School of Geography and Earth Science, you all make grad school that much better in the long-run.

To all the other professors that have helped me grow individually during my studies:
Dr. Mark Smith for sparking my interest in the geomorphological world around us and thus my route of study.
Dr. Owen Hertzman for seeing a potential young hydrologist in me, may he rest in peace.
Dr. Dan Gibson and Dr. Derek Thorkelson for offering a geography student the opportunity to branch out into the world of structural geology.
Dr. Gwenn Flowers for introducing me to the field of hydrogeology.

A whole hearted thanks goes to my family for their endless and unconditional love, support, and encouragement.

Finally, thanks to my partner in crime, Genevieve Jin and her family for their continual support throughout my academic journey and in all aspects of life. I truly could not have done it all without Genevieve by my side, it is because of her that I even made the decision to attend post-secondary, 고마워 많이 사랑해요.

Table of Contents

List of Figures

Chapter 1

Chapter 2

Chapter 3

List of Tables

Chapter 3

Chapter 1: Introduction

1.1 Introduction

Alpine streams are an important component of the hydrological cycle, draining landscapes, and connecting water bodies for distribution and storage of surface water. Stream ecosystems provide crucial habitat to organisms, playing an integral role in their survival. Stream temperature is a primary control on biogeochemical conditions such as dissolved oxygen and nutrient cycling (Kelleher et al., 2012), and is a major subject of research globally due to its susceptibility to climate change (Brown and Hannah, 2008). The thermal regime of a stream is defined as the observed spatiotemporal patterns of water temperature variations (Caissie, 2006).

Stream thermal regimes are influenced by the exchange of water and energy across the stream surface, banks, and bed (Figure 1.1). This includes atmospheric heat exchange through radiative and turbulent transfers, and advection of heat from groundwater and tributary inputs (Kelleher et al., 2012). The balance of these fluxes is referred to as the energy budget of a stream and is of primary interest to researchers for its use in assessing the potential impacts of anthropogenic activity and climate change on stream temperature (e.g., Mayer, 2012; Moore et al., 2005). The complex spatiotemporal variations of these elements are a primary reason for the ongoing difficulty in understanding and forecasting their behaviour at regional scales, and thus the importance of continued study (Kelleher et al., 2012). Further, the establishment of localized cold water areas in streams result in thermal refugia which are key for the survival of cold-water fish species during high summer temperatures (Dugdale et al., 2013). On longer time scales, these reaches within streams can be identified as climatic refuges, areas where cold water organisms can persist during ongoing climate change (Harrington, 2017; Isaak et al., 2015).

Climate change increases the need for study of thermal regimes in northern alpine streams as most projections agree that the greatest warming in the future will be experienced at high latitudes and altitudes (DeBeer et al., 2016; Pepin et al., 2015). This is important in Canada as many of the largest rivers flow through the permafrost region above 60˚ N (Environment and Climate Change Canada, 2013). An important consideration in a warming climate is the thermal sensitivity of a stream, defined as the sensitivity of a stream to changes in air temperature (Kelleher et al., 2012). This is notable as there is much documented evidence of long-term increases in stream temperatures associated to climate change (e.g., Arora et al., 2016; Hari et al., 2006; Mayer, 2012). With increasing stream temperatures under future climate change there is a risk of losing the above mentioned thermal refugia offered by alpine streams, thus posing a threat to cold-water fish species and biogeochemical cycling in these systems. Therefore, we must improve our understanding of the thermal regimes of alpine streams and their sensitivities to future climate change. This will help to prevent potential ecosystem degradation, and sustain regional hydrological and ecological systems that rely on these crucial conduits.

1.2 Alpine permafrost hydrology

Snowfall is a significant component of the hydrological cycle in Canada, accounting for up to 80% of total precipitation in some areas (Marsh et al., 1990). Snowcover plays a large control on the surface energy balance, impacting the degree of freezing that a soil will experience and thus the distribution of permafrost and seasonally frozen ground in these regions (Zhang et al., 2003). Permafrost is defined as ground that remains continuously frozen ($\leq 0^{\circ}C$) over periods greater than two years (Brown and Kupsch, 1974). This perennially frozen ground acts as a largely impermeable substrate, affecting the hydrology of regions by controlling the distribution, quality, and supply of groundwater (Prowse et al., 1990). This is important to the hydrology of Canada, as more than half of its landmass is underlain by zones of continuous and discontinuous

permafrost (Brown, 1970). The strong hydraulic isolation imposed by permafrost results in complex connections between permafrost aquifers and streams in these areas.

Generation of streamflow in permafrost basins is distinct from temperate ones as: 1) snowmelt is the most important hydrologic event of the year, 2) where permafrost exists, deep recharge to subpermafrost aquifers is restricted, and 3) if present, the organic active layer provides suprapermafrost water with swift paths for discharge to streams (Carey et al., 2013). The active layer is the region above permafrost that is seasonally frozen or thawed, altering its permeability over the year. This results in throughflow, infiltration, recharge, and discharge being either promoted or restricted (Ge et al., 2011). Due to seasonal freeze-thaw cycles, aquifers located in the active layer above the permafrost play a primary role in contributing to streamflow in these regions (Woo, 2012), controlling response to snowmelt and summer precipitation (Walvoord and Kurylyk, 2016). With increased warming and degradation of permafrost, it is predicted that the flow regimes of these streams will become altered. Increased air temperature will affect soil temperatures, consequently disrupting surface water-groundwater flow regimes, and changing the quality and quantity of water in these regions (Okkonen et al., 2010). With thawing permafrost, the active layer will become thicker in subsequent years, allowing for prolonged pathways for discharge. These potential changes will result in modifications to stream runoff response (Carey et al., 2013), and the possibility of increased stream temperatures.

The controls that permafrost and snowmelt exert on streamflow in alpine watersheds can be seen in their streamflow hydrographs. These basins have pronounced freshets dominated by spring snowmelt, providing most of their discharge at this time. They are further characterized by low winter flows fed by groundwater discharge and similarly low flows in late summer, with large peaks in response to rainstorms (Woo et al., 1990; Woo, 2012). With greater amounts of

permafrost, streams will display a much flashier response to snowmelt and summer precipitation due to increasingly retarded infiltration (Hinzman et al., 2005). Groundwater discharge during winter is often unable to contribute to baseflow, as much of the discharge freezes, creating icings or aufeis at points of discharge (van Everdingen et al., 1990). This can result in smaller rivers having zero flow during the winter (Hinzman et al., 2005). With decreasing amounts of permafrost, basins become more responsive to infiltration, allowing for greater recharge and higher seasonal baseflows (Hinzman et al., 2005).

1.3 Surface water-groundwater interactions

The hyporheic zone is the area along the margins of a stream through which surface water-groundwater interactions occur through the streambed sediment (Figure 1.2) (Gooseff, 2010). This results in transient storage due to the notably slower travel times through this zone compared to in-channel flow. These differences in flow rate result in a range of stream water residence times and contribute to unique ecological conditions within the stream by allowing for extended interactions with microbial communities (Boano et al., 2014; Zarnetske et al., 2007). Hyporheic exchange is important for the overall health of a stream ecosystem as it promotes nutrient cycling and acts to increase levels of dissolved oxygen. This increases overall productivity and contributes towards the survival of various streambed organisms (Gooseff, 2010).

Aquifers in permafrost regions are classified based on their position: 1) suprapermafrost aquifers occur in the active layer above the permafrost table, 2) intrapermafrost aquifers are not subjected to seasonal freezing and are often found in unfrozen windows (taliks), and 3) subpermafrost aquifers occur below the permafrost (Figure 1.3) (van Everdingen et al., 1990). These aquifers occur in all types of geology with varying connections between them and surface water bodies (van Everdingen et al., 1990). In continuous permafrost areas, most subsurface flow

is comprised of suprapermafrost water through the seasonally thawed active layer (Woo, 2012), restricting shallow groundwater discharge to the summer season. As it acts as a year-round, semi-permanent aquiclude (Hinzman et al., 2005), permafrost in many northern regions plays a large role in the amount of water exchange across the stream boundary. In areas of continuous permafrost, this can be entirely dependent on the depth of permafrost thaw beneath the stream channel, as permafrost can surround the entire channel margin (Zarnetske et al., 2007).

Stream morphology plays a role in controlling the distribution of hyporheic zones, and the rate and magnitude of fluxes through them (Zarnetske et al., 2007). At the local scale, zones of water exchange are often established due to differences in hydraulic head, created by meander bends and pool-riffle complexes. In general, water will downwell and upwell at areas of high and low head, respectively (Figure 1.4) (Malard et al., 2002). Permeability of bed sediment also affects exchange zone distribution, with water downwelling in areas of high permeability, and upwelling downstream as permeability decreases (Malard et al., 2002; Zarnetske et al., 2007). The interplay of morphology and permeability allows for a priori identification of potential zones of exchange. However, as channel morphology and sediment permeability are affected by flood cycles, the location and extent of surface water-groundwater exchange zones can be dynamic throughout a season (Malard et al., 2002).

1.4 Stream temperature

1.4.1 The energy budget of a stream

Modelling stream energy budgets is frequently used in assessing the dominant contributing fluxes to stream thermal dynamics and the potential impacts of climate and land use change (e.g., Leach and Moore, 2010; Magnusson et al., 2012). Although the standard configuration of the energy budget of streams is well defined, the method of calculation and included components will vary with the environment, data availability, and season in question

(e.g., Glose et al., 2017; Moore et al., 2005; Westhoff et al., 2007). A general form of the energy budget for a defined stream reach is (Moore et al., 2005):

$$\frac{dS}{dt} = \text{(distributed fluxes)} + \text{(longitudinal advection)} + \text{(lateral advection)} \quad (1)$$

$$\frac{dS}{dt} = wL(\Phi_{net} + \Phi_{latent} + \Phi_{sens} + \Phi_{bed} + \Phi_{fric}) + \Delta Q_{aL} + \Delta Q_{aS} \quad (2)$$

Where $\frac{dS}{dt}$ represents the rate of change in energy storage (W) in the reach, w is average stream width (m), L is reach length (m), Φ_{net} is net radiation (W/m^2), Φ_{latent} is latent heat flux (W/m^2), Φ_{sens} is sensible heat flux (W/m^2), Φ_{bed} is streambed conduction, (W/m^2), Φ_{fric} is frictional heating (W/m^2), ΔQ_{aL} is net longitudinal advection along the stream (W), and ΔQ_{aS} is streambed lateral advection (heat advection due to groundwater, W).

1.4.1.1 Distributed energy fluxes

Net radiation (Φ_{net}) reaching the surface of a stream is the sum of shortwave (Φ_{SW}, W/m^2) and longwave radiation (Φ_{LW}, W/m^2):

$$\Phi_{net} = \Phi_{SW} + \Phi_{LW} \quad (3)$$

Total shortwave radiation reaching a stream (Φ_{SW}) can be determined by correcting measured incoming shortwave radiation (Φ_{Sdown}, W/m^2) for channel shading (SF; 0 to 1, direct versus diffuse insolation, respectively, determined either qualitatively or quantitatively) and assuming a standard albedo (0.05) for the stream surface (Glose et al., 2017; Leach and Moore, 2017; Magnusson et al., 2012):

$$\Phi_{SW} = (1 - albedo)(1 - SF)(\Phi_{Sdown}) \quad (4)$$

Net absorbed longwave radiation (Φ_{LW}) is determined as the sum of incoming longwave radiation (Φ_{Lin}, W/m^2), emitted longwave radiation from the stream surface ($\Phi_{emitted}$, W/m^2), and longwave radiation from landcover to the stream (Φ_{LC}, W/m^2) (Glose et al., 2017):

$$\Phi_{LW} = \Phi_{Lin} + \Phi_{emitted} + \Phi_{LC} \quad (5)$$

If atmospheric longwave radiation (Φ_{down}, W/m^2) is directly measured, incoming longwave radiation (Φ_{Lin}) can be determined by correcting for vegetation through use of the view-to-sky factor (*vts*; 0 to 1, full canopy versus no canopy, respectively, determined either qualitatively or quantitatively):

$$\Phi_{Lin} = \Phi_{down} vts \quad (6)$$

Both longwave radiation emitted from the stream surface ($\Phi_{emitted}$) and landcover (Φ_{LC}) are calculated according to the Stefan-Boltzmann law as a function of the emissivity of water (ε, 0.96) and measured water or air temperature (Boyd and Kasper, 2003; Glose et al., 2017):

$$\Phi_{emitted} = -0.96\sigma(T_w + 273.2)^4 \quad (7)$$

$$\Phi_{LC} = 0.96(1 - vts)0.96\sigma(T_{air} + 273.2)^4 \quad (8)$$

where σ is the Stefan-Boltzmann constant (5.67×10^{-8} W/m^{2}K^4), T_w is water temperature (˚C), and T_a is air temperature (˚C).

Latent heat flux (Φ_{latent}, W/m^2) is the energy used for either condensation or evaporation and is calculated using the estimated evaporation rate (*E*, mm/d), water density (ρ_w, kg/m^3), and the latent heat of vapourisation of water (L_v, J/kg; Glose et al., 2017):

$$\Phi_{latent} = -\rho_w L_v E \quad (9)$$

The latent heat of vapourisation of water (L_v) will change with water temperature:

$$L_v = 10^6\times(2.501\text{-}0.002361T_w) \quad (10)$$

Evaporation (*E*) is commonly calculated using a mass transfer approach (Dingman, 2002):

$$E = (1.505\times10^{-8}+1.6\times10^{-8}u)(e_w - e_a) \quad (11)$$

where the empirically determined constants are dependent on the height at which windspeed (*u*, m/s) and vapour pressure (e_a, kPa) are measured (2 m height in this formulation).

e_w is the saturation vapour pressure of the evaporating surface (kPa):

$$e_w = 0.61\, exp\left(\frac{17.27T_w}{237.3+T_w}\right) \quad (12)$$

Air vapour pressure (e_a) is:

$$e_a = \frac{RH}{100} e_s \quad (13)$$

where RH is relative humidity and e_s is saturation vapour pressure (kPa):

$$e_s = 0.611e^{\left(\frac{17.27T_{air}}{237.3+T_{air}}\right)} \quad (14)$$

Sensible heat flux (Φ_{sens}) is the transfer of energy between air and the stream surface and is often calculated using the Bowen ratio (B_r) and latent heat flux (Φ_{latent}) (Glose et al., 2017):

$$\Phi_{sens} = B_r \Phi_{latent} \quad (15)$$

where the Bowen ratio (B_r) is (Dingman, 2002):

$$B_r = \gamma\left(\frac{T_w - T_a}{e_w - e_a}\right) \quad (16)$$

where γ is the psychrometric constant (kPa/K), calculated using adiabatic air pressure.

Streambed conduction (Φ_{bed}) is heat transferred between the streambed and water (Boyd and Kasper, 2003), and can be calculated via Fourier's law (Moore et al., 2005):

$$\Phi_{bed} = \frac{K(T_b - T_w)}{0.05\ m} \quad (17)$$

where K is the effective thermal conductivity of the streambed (W/m˚C), and T_b is streambed temperature at 0.05 m below the bed.

Frictional heating (Φ_{fric}) is calculated with the standard equation of Theurer et al. (1984):

$$\Phi_{fric} = \frac{g\Delta z \rho_w Q}{Lw} \quad (18)$$

where g is the gravitational constant (m/s^2), Δz is change in stream elevation (m), Q is stream discharge at the outlet (m^3/s), L is reach length (m), and w is mean channel width (m).

1.4.1.2 Advective energy fluxes

Advective energy fluxes affect the energy budget of a stream by adding or removing thermal mass along the reach (Kurylyk et al., 2016). Longitudinal advective heat flux (ΔQ_{aL}, W) through a stream reach can be calculated as (Harrington, 2017):

$$\Delta Q_{aL} = C_w(Q_u T_u - Q_d T_d) \quad (19)$$

where C_w is the volumetric heat capacity of water (4.18×10^6 J/m^{3}K), Q is discharge (m^3/s), T is stream temperature (˚C), and the subscripts u and d indicate sampling at the upstream and downstream boundaries, respectively.

1.4.2 Thermal regimes of northern rivers

Stream temperature varies seasonally, with temperatures decreasing in winter and increasing in summer. As the temperature of snowmelt is at 0˚C, alpine, nival dominated streams are initially cooled as air temperatures rise due to increased snowmelt input (Leach and Moore, 2014; Lisi et al., 2015). Upon the completion of seasonal snowmelt, stream temperature will begin to increase with increasing air temperatures and inputs from rainfall. This damped response of stream temperature to increasing air temperatures is commonly observed in alpine streams. By comparison, streams in pluvial dominated catchments have been found to be 5 to 8 times more sensitive to variations in surface energy exchanges during summer than that of streams of the nival regime (Lisi et al., 2015).

1.4.3 Groundwater influences

The thermal regime of a stream is influenced by the amount and temperature of groundwater discharge (Mayer, 2012). This, as well as the hyporheic flowpath can cause variations in temperatures along the streambed at areas of upwelling, altering the streams response to diel temperature variations. Water upwelling from short flowpaths will resemble that of stream water in its daily mean temperature but will have a distinct diel range, damping the diel stream temperature range at that location. In comparison, water upwelling from longer flowpaths

will have a distinct diel temperature range and mean daily temperature (Poole et al., 2008). Therefore it will be cooler or warmer than stream water in summer or winter, respectively, which can modify the mean daily stream temperature (Evans and Petts, 1997; Poole et al., 2008). As previously mentioned, upwelling of cooler water to streams is also important in establishing local thermal refugia for cold-water species during times of elevated stream temperatures (Dugdale et al., 2013).

1.4.4 Permafrost influences

Near the headwaters of groundwater fed streams, temperature is often close or equal to that of its source, with temperature increasing with distance downstream (Caissie, 2006). As permafrost is characterized by temperatures at or below 0˚C (Brown and Kupsch, 1974), it can be assumed that the temperature of upwelling groundwater in these regions will be quite low. However, as most groundwater discharge in permafrost regions comes from suprapermafrost aquifers within the shallow active layer (Woo, 2012), the temperature of water inputs will increase with rising air temperatures over the summer season (Mayer, 2012)

1.4.5 The state of the science

As factors influencing stream thermal regimes show large spatiotemporal variability, there is a limited process based understanding of the controls to water temperature and variability in headwater catchments (Khamis et al., 2015). Numerous recent studies have investigated changes in stream temperature as a result of energy exchanges across the stream surface, bed, and banks, thus documenting the distinct characteristics of alpine stream thermal regimes (e.g., Khamis et al., 2015; Leach and Moore, 2017; Webb et al., 2008). Likewise, many studies have been conducted on rivers and streams in permafrost basins (e.g., Ge et al., 2011; Maclean et al., 1999) due to the threat held by future climate change to thawing permafrost (Okkonen et al., 2010). However, most have typically focused on resultant changes in surface and subsurface

water fluxes, stream biogeochemistry, and the permafrost-carbon feedback (Walvoord and Kurylyk, 2016). Studies conducted in permafrost basins that focus on the stream thermal dynamics and energy exchange are often done on much larger river systems (e.g., King et al., 2016; Yang et al., 2014). Thus, a knowledge gap exists regarding the stream thermal dynamics of permafrost underlain alpine watersheds.

1.5 Objectives

Water temperature and variability in permafrost underlain headwater streams is poorly documented, yet has important ecological and biogeochemical implications in a changing climate (Caissie, 2006; Gooseff, 2010). Due to their low temperatures, the thermal regimes of alpine streams are distinctly important in studies of climate change as they commonly offer thermal and climatic refugia for cold-water aquatic species (Dugdale et al., 2013; Harrington, 2017; Isaak et al., 2015). The overall purpose of this study is to determine the distinctive characteristics of alpine stream thermal regimes and the influence of respective heat fluxes. Specific objectives are to (1) identify and describe the spatiotemporal thermal patterns in two alpine streams underlain by discontinuous permafrost, and (2) quantify the dominant energy fluxes contributing to these patterns through an energy budget approach. Based on the identified spatiotemporal trends, a special focus will be given to the perceived influence of groundwater within each catchment.

Chapter 2: Study Site Characterization and Methods

2.1 The Wolf Creek Research Basin

The Wolf Creek Research Basin (WCRB, 60˚31’40” N, 135˚31’14” W) is an alpine basin (195 km^2) underlain by discontinuous permafrost, located 15 km southeast of Whitehorse, Yukon Territory. The WCRB was established in 1993 as a long-term watershed research project and consists of three different ecological zones: boreal forest, subalpine shrubland, and alpine tundra. Regional climate is classified as subarctic continental, represented by a wide temperature range

and low precipitation (Carey and Quinton, 2005). The average (1981-2010) annual air temperature at the Whitehorse International Airport (706 m.a.s.l.) is -0.1˚C, ranging from -15.2˚C (January) to 14.3˚C (July). Average annual precipitation is 262.3 mm, 61 % of which falls as rain (Environment and Climate Change Canada, 2017). However, due to orographic factors, precipitation in the WCRB is approximately 25 % – 35 % greater (Pomeroy et al., 1999). The focus of this study is on the Granger Creek (GC) and Buckbrush Creek (BB) sub-basins (Figure 2.1), both of which are headwater catchments of similar area (GC: 7.6 km^2, BB: 6.1 km^2) and exist within the subalpine-alpine transition zone of the WCRB. Both GC and BB have a similar elevation range (GC: 395 m, BB: 365 m) and total flow length (GC: 4.8 km, BB: 3.8 km). Each creek has a common west-east flow direction and bed sediment consisting of boulders, cobbles, and gravels, with limited sandy deposits. These similarities between each stream facilitate inter-comparison for this study. The underlying geology of the GC and BB basins is predominantly sedimentary, and includes limestone, siltstone, sandstone, and conglomerate; overlain by till. Permafrost underlies much of the north-facing aspects and seasonal frost is dominant in the south-facing slopes. Primary vegetation throughout the basins are various willow shrubs (*Salix*), alder shrubs (*Alnus*), and Labrador tea (*Ledum groenlandicum*), with sparse stands of white spruce (*Picea glauca*) (Carey and Quinton, 2005; McCartney et al., 2006). With increasing elevation, vegetation transitions from primarily shrubs in valley bottoms to tundra foliage in uplands. The hydrogeologic environment of these basins is not thoroughly characterized, but geophysical surveys in the WCRB identified primarily low hydraulic conductivites (10^{-6} m/s) of aquifers, with groundwater discharge feeding creeks in the alpine zone (Seguin et al., 1999). This study focuses on a 1950 m reach of each stream possessing similar channel characteristics. The upper study reaches of each stream are narrower, slightly

meandering channels with little shading from vegetation, while the lower portions are more shaded, wider, and have a step-pool morphology (Figure 2.2). The study reaches of GC and BB have elevation ranges of 137 m (7% gradient) and 175 m (9% gradient), respectively. Both reaches are influenced by tributaries, GC having two, flowing in at 1100 m and 1350 m downstream; while the tributary to BB flows in at 1550 m downstream (blue arrows, Figure 2.3).

2.2 Methods

2.2.1 Field Methods

The study period spanned the summer field season from June to September, 2016. Water temperatures were recorded at a 15-minute frequency using iButtons (model iBWetLand DS1922L, precision of ±0.5˚C, resolution of 0.0625˚C). In total, 40 iButtons were used in each stream (yellow points, Figure 2.3), with one installed centre-channel at the sediment-water interface every 50 m along the length of each study reach (Figure 2.4). At each location, a steel bar was driven into the bed and a sensor was fixed to the bar at the streambed. The location of the first sensor in each creek was chosen to be just upstream (~5 m to 10 m) of pre-established hydrometric stations (yellow triangles, Figure 2.3). Successive sensor locations were then measured out with a tape measure while travelling upstream. During installation, water depth, bed sediment, and shading/vegetation height were also recorded. iButton downloads were performed minimally to preserve data continuity, resulting in three instances over the observation period (approximately every five weeks).

Vertically spaced streambed temperature time-series were collected by mounting iButtons in survey stakes and driving them into the bed to record temperature at depths of 0.05 m and 0.15 m below the sediment-water interface. A 30-minute recording frequency was used for these time-series to ensure recording over the full June-September season without need for removal and download. This was done to reduce destruction of the vertical sediment structure and allow full

recording during the observation period. These were then installed (five in GC four in BB) at locations chosen a priori (pool-riffle complexes or point bars with predominantly coarse sediment; blue stars, Figure 2.3) to maximize the likelihood of recording an upwelling/downwelling induced temperature gradient (Malard et al., 2002).

To approximate groundwater temperature, riparian wells on either bank of each stream (north-facing and south-facing; red points, Figure 2.3) were instrumented with Solinst LTC (Level, Temperature, Conductivity) Levelogger Edge pressure transducers, recording at 15-minute frequencies. Pre-existing wells in GC were utilized, while new wells were installed on either bank of BB near the study reach outlet. Wells were 50.8 mm (internal diameter), 1.8 m long perforated ABS piping with screened sections along the entire subsurface lengths, hand-augured to a depth of -0.75 m.

Hydrometric stations were established at best possible locations (channel mostly straight, uniform depth, no obstructions immediately upstream) along the length of each creek in order to account for discharge change with distance due to tributary inflow and groundwater-surface water exchange (green triangles, Figure 2.3). Stilling wells were installed using 50.8 mm (internal diameter) ABS pipe mounted to steel t-posts that were driven into the bed. These were instrumented with Solinst LTC Levelogger Edge pressure transducers, recording at 15-minute frequencies. Staff gauges were attached to the stilling wells to record stage during manual discharge measurements. In total, five and three stilling wells were installed along GC and BB, respectively. Manual discharge was measured using a SonTek FlowTracker handheld Acoustic Doppler Velocimeter and the velocity-area method (Dingman, 2002). This was done at the 'outlet' of each study reach 16 times over the study period, approximately once per week. For stations established further upstream in each creek, manual discharge measurements were done

five times over the study period (once in June, August, and September; twice in July). Due to a lack of hydrometric data in the uppermost reach of BB, a slug injection salt dilution was performed at the end of the season (Dingman, 2002). This was done at the location of the topmost temperature sensor over a 57 m reach, as well as at the outlet over a 39 m reach using 100 g of salt, dissolved in 1 L of water, and logging every 5 seconds with a YSI Multiparameter Sonde.

Stream surveys using a YSI Sonde were performed several times over the study period in each stream (seven in GC, five in BB). Measurements were taken at each temperature sensor location and temperature, conductivity, and specific conductivity were recorded to offer comparison with iButton temperatures and identify other relevant trends. Leaf Area Index (LAI) was measured at each sensor location using a LI-COR Plant Canopy Analyzer (LAI – 2200C) during a survey in July. Upward facing photos were taken at sensor locations using a GoPro Hero3 camera for comparison with LAI measurements.

Climate data were collected with established weather stations located within the research basin (red triangles, Figure 2.3). Along with other parameters, the weather stations measured incoming and outgoing shortwave and longwave radiation (Kipp & Zonen, CNR4), relative humidity and air temperature (Campbell Scientific, HMP45C-L), and wind speed (RM Young) at 30-minute intervals. Precipitation (Geonor, T-200B) was also recorded throughout the year at several locations within the WCRB.

2.2.2 Data Analysis

As field data was collected over varying time periods, all analyses were performed for the time period of June 22 to September 5, 2016 to ensure concurrence. Longitudinal temperature time-series (i.e., temperature vs. distance relationship for each 15-minute interval) were first compiled for each stream to facilitate investigation of the thermal regime and all subsequent

analyses using MATLAB (The Mathworks Inc., 2016). Specific conductivity values from stream surveys were also plotted longitudinally for comparison with identified trends in water temperature. Additionally, daily maximum, minimum, and mean water temperatures were extracted and plotted with seasonal values in order to identify trends and variations within and between the streams.

Linear regressions between mean daily air and water temperatures at each stream temperature sensor location were performed to identify the empirical relationships between water and air temperatures. This approach is used to discern groundwater influence within streams, as groundwater-dominated watersheds tend to have low regression slopes with relatively high intercepts, while runoff-dominated streams display steeper slopes with intercepts closer to 0˚C (Figure 2.5) (Caissie, 2006). Linear regression also helps determine the stream thermal sensitivity, as low (high) regression slopes indicate low (high) sensitivity (Mayer, 2012). The regression slope and intercept values for each temperature sensor location were then plotted longitudinally to identify spatial trends of the correlation coefficients and for comparison with longitudinal profiles of water temperature. Cross-correlations between water and streambed temperatures, and water temperature variance were computed to obtain a measure of stream thermal characteristics.

To prepare discharge data for use with the energy budget, all levelogger readings from hydrometric stations were first corrected for atmospheric pressure using a Solinst Barologger located within the watershed. A stage-discharge curve was created for each station through manual measurement over the study period. Upon correction for offset between manual and levelogger stage, the equation of this curve was applied to convert continuous levelogger stage to stream discharge. Additionally, the levelogger used at the outlet location (BCQ) in BB failed

during the season, requiring reconstruction of stream discharge at that station. This was done by identifying the average offset between manually measured values of stream discharge at BCQ and the next station upstream (BCQ1) and then adding it to the high frequency discharge data at BCQ1 to estimate flow at BCQ. A similar exercise was performed using salt dilution data to estimate continuous flow at the uppermost reach of BB.

View-to-sky (*vts*) and the complementary shading factor (*SF*) for each temperature sensor location was computed from both LAI values and upward facing GoPro photos taken during stream surveys (Figure 2.6). Values calculated from the LAI relation (Rasmus et al., 2013) were less representative of field estimations and thus values calculated from GoPro photos using a custom MATLAB (The Mathworks Inc., 2016) function were used with the energy budget. This function applies successive filters to the RGB colours in a photo to mask bright regions and then calculates *vts* from the remaining dark areas. All data from weather stations were resampled using linear interpolation to obtain 15-minute intervals, ensuring continuity with stream temperature and discharge data.

The Vertical Fluid Heat Transfer Solver (VFLUX 2; Gordon et al., 2012; Irvine et al., 2015) was used to determine rates of upwelling and downwelling at the locations of the vertical streambed profiles. This software package automates the analysis of streambed temperature time-series to examine how diel surface water temperature signals are damped and lagged with depth. This analysis yields an estimate of the direction and magnitude of the vertical water flux through the sediment, as the diel temperature signal damping and lagging is dependent on the vertical flow characteristics. For a full discussion of the flux calculation methods by VFLUX 2, refer to Gordon et al. (2012), and Irvine et al. (2015). Additionally, the one-dimensional transient stream temperature model HFLUX (Glose et al., 2017) was used to simulate water temperature over the

instrumented reach of each stream. This analysis provides an independent method to estimate groundwater-surface water exchange, as groundwater inflow will influence changes in the stream discharge (estimated via differential stream gauging) and stream temperature.

2.2.3 Energy Budget Construction

To facilitate understanding of the spatiotemporal trends observed within these stream systems, an energy budget was constructed in MATLAB (The Mathworks Inc., 2016) using equations 1 – 19 outlined in Chapter 1.

Distributed energy fluxes were determined for each water temperature monitoring location along the study reach of each stream. These values were then averaged over each reach to facilitate understanding of calculated fluxes over the study period. The energy budget formulation for this study considers net radiation and turbulent fluxes positive downwards, streambed conduction and frictional heating positive upwards, and longitudinal advection positive into the study reach. There is error associated with the use of (15) for calculation of sensible heat flux, as when humidity nears 100%, B_r approaches infinity; however, as humidity rarely approached 100% during the study period, this method was deemed sufficient. To determine streambed conduction (17), effective thermal conductivity was assumed to be 2.5 W/m˚C for cobbles (Glose et al., 2017). There is large uncertainty with (18) in that it assumes all gravitational potential energy is converted into frictional heating, neglecting energy dissipated through other means such as turbulence and sediment transport. Further, it is noted by Hannah et al. (2008) that this formulation produced unrealistically high values in a similarly steep stream. Thus, although frictional heating is considered in this energy budget, it is used with caution.

Due to difficulty quantifying the complex spatiotemporal variability of groundwater-surface water interactions along the study reaches, streambed lateral heat advection (ΔQ_{aS}, W) was unable to be determined. Further, as there was a lack of measurement of tributary discharge,

lateral advective heat flux from the discharge of a tributary is also unknown. Thus, these unknowns are grouped together into a single lateral advective heat flux term and left as an unknown variable, ΔQ_{aS}.

Chapter 3: Results

3.1 Climate

Air temperature in WCRB was slightly cooler than regional climate normals, while precipitation was variable but higher overall during the study period (June – September 2016). Total precipitation received over the 4-month period was 157 mm, approximately 12.5 % greater than the long-term (1981-2010) average of 139.6 mm at the Whitehorse International Airport (Environment and Climate Change Canada, 2017). Precipitation over the study period was reasonably consistent, with 33 % (52.3 mm), 17 % (28.5 mm), 27 % (40.2 mm), and 23 % (36 mm) of total falling in June, July, August, and September, respectively. Each month experienced a large rain event that accounted for the majority of monthly precipitation (Figure 3.1). In June, 56 % (29 mm) of total monthly precipitation fell over a 2-day period (June 13 – 15). Rain during July 14 – 15 accounted for 50 % (13 mm) of total monthly precipitation. August received 51 % (22 mm) of its total monthly precipitation during a large storm on August 26. Finally, 82 % (29 mm) of monthly precipitation in September fell during the 2-day period of September 9 – 10. The mean daily air temperature (9.9˚C) during the observation period was cooler than regional climate normals by 1.7˚C (Figure 3.2).

3.2 Stream hydrographs

Mean June – September stream discharge at the study reach outlets of each stream was approximately equal (0.13 m^3/s), showing a strong response of each stream to large early season precipitation inputs due to the presence of frozen ground increasing runoff (Figures 3.1 and 3.3a). Over the study period, the patterns of flow for GC and BB were distinct. Early in the

period, GC had greater flow than that of BB, while BB had flow greater than GC from mid-study period onward. A clear diel discharge signature was observed, created by the response of each stream to variation in diurnal snowmelt (Carey et al., 2013) or evapotranspiration (Schwab et al., 2016). Flow along the study reaches of each stream also had distinct characteristics (Figure 3.3b). Discharge along BB increased only slightly along the first 1600 m downstream before the inflow of its tributary, which resulted in a 43.7 % increase in discharge between gauging stations. GC displayed a losing section along the first 335 m downstream (25.8 % decrease in flow) before increasing only slightly until the inflow of its tributary at 1150 m downstream, resulting in an increase in discharge of 34.5 % between gauging stations.

3.3 Spatiotemporal trends

3.3.1 Spatial cooling and response to tributaries

Dense thermal monitoring of each stream resulted in comprehensive spatiotemporal plots of stream temperature development over the study period (Figure 3.4). The length of observation captured both the warming and cooling period over the summer season, which was punctuated by three distinct warming events (Figure 3.5a) that coincided with substantial precipitation events (Figure 3.1). Seasonal temperature plots showed that each stream exhibited a low diel amplitude (1.5˚C and 1˚C in GC and BB, respectively), with BB being consistently ~1˚C cooler than GC (Figure 3.5b). Longitudinal temperature plots revealed high thermal heterogeneity in each stream, highlighting areas of consistent temperature decrease along the length of each stream (specifically, 100 m, 400 m and 750 m, and 50 m, 500 m and 850 m downstream from the uppermost monitoring location in GC and BB, respectively). These plots further illustrated the differing response of each stream to tributaries, with GC warming due to tributary inflow at 1150 m and 1450 m downstream, while BB cooled from inflow at 1600 m downstream (Figures 3.5a and 3.6). Each stream also displayed a distinct trend in overall downstream behaviour of

temperature, GC warmed slightly, while BB first warmed, then cooled with distance downstream (Figures 3.6 and 3.7).

Longitudinal plots of specific conductivity (SpC, µS/cm) in each stream had similar trends to longitudinal temperatures. In GC, SpC increased slightly (~2 µS/cm – 5 µS/cm) at 100 m, 400 m, and 750 m downstream, while markedly increasing (~10 µS/cm) at 1150 m downstream. This corresponded to the observed locations of persistent temperature decrease as well as primary tributary inflow (Figure 3.8). This pattern was observed in BB, where SpC increased slightly (~2 µS/cm) at 50 m and 500 m downstream, and increased substantially (~20 µS/cm) at 850 m downstream. Conversely, SpC in BB decreased (~2 µS/cm) in response to tributary inflow at 1600 m downstream (Figure 3.9).

3.3.2 Linear regressions and spatiotemporal variance

Linear regressions between mean daily air and water temperatures produced low regression slopes with relatively high intercepts along the length of each stream. Locations with noticeably lower slope and higher intercept values for daily mean air and water temperature regressions were consistent with locations along the length of each creek that consistently displayed decreases in water temperature (Figures 3.6, 3.10 and 3.11). Averaged over the reach length, the streams shared a common mean regression slope (0.37); however, the mean intercept of BB (2.1˚C) was nearly a full degree higher than that of GC (1.2˚C). With distance downstream, each stream had a decrease in regression slope and an increase of intercept. Over the 1950 m study reach, regression slope (intercept) in GC went from 0.37 (1.2˚C) at the upstream location to 0.33 (2.6˚C) at the outlet location. Similarly, in BB regression slope (intercept) went from 0.37 (2.1˚C) upstream to 0.24 (3.3˚C) downstream. BB showed considerably lower regression slopes and higher intercepts with distance downstream than was observed in GC.

Longitudinal plots of temperature variance at each sensor revealed an overall decrease with distance downstream for GC. BB showed both increases and decreases in the upper reach, with an overall decreasing trend before increasing slightly towards the outlet from 1300 m downstream (Figure 3.12a). Spatial variance corresponded well with observed increases and decreases in water temperature, as well as tributary input along each stream (Figures 3.12a and 3.6). The pattern in spatial temperature variance also followed that of longitudinal water temperature more closely in BB than GC. Temporal temperature variance over each reach for the study period showed distinct behaviour in the trends of each stream (Figure 3.12b). GC exhibited considerably higher temperature variability throughout the study period, while each stream showed contrasting trends in increases and decreases of variance. Often temperature variance in BB was at its lowest, while that of GC was near its highest values.

3.3.3 Thermal response and temperature lags

The thermal response of each stream was determined by examining the timing of temperature maxima and minima at each sensor location in relation to inputs of precipitation and shortwave radiation. This revealed a clear synchroneity in the thermal response of each stream to peak incoming shortwave radiation, with temperature maxima at each sensor location typically occurring within 15 minutes of each other (Figure 3.13). Evaluating diel trends in the relation between air and water temperature revealed noticeable lags between the respective daily temperature maximums. However, an unexpected observation was the frequent occurrence of a negative lag, indicating that stream temperature reached its daily maximum value prior to that of air temperature (Figures 3.14 and 3.15). Typically, a negative lag occurred during very warm periods, while positive lags (air temperature peaking first) occurred during cooling periods. This phenomenon occurred frequently throughout the season along the length of each stream (Figure 3.16). To further investigate this event, a comparison was done between net radiation received by

the streams and water temperature (Figure 3.17). This showed that a negative lag also occurred between net radiation and water temperature, however this did not occur as frequently as the negative lag between air and water temperature (Figure 3.18). Further, even with a negative air-water temperature lag, peaks in net radiation still led that of water temperature in some instances.

3.3.4 Vertical temperature profiles

Vertical streambed temperature profiles were used to establish whether downwelling was occurring within the streams. Through efficient downward propagation of the diel temperature signal into the sediment, zones of downwelling were identified at these locations within each stream (Figure 3.19a). Downwelling conditions encourage efficient downward propagation of diel temperature signals due to thermal conduction and advection acting in parallel (Irvine et al., 2017) (Figure 3.19b). This was supported by cross-correlation of water and streambed sediment temperature, which resulted in high coefficient of determination values (0.996-1) and low lag times (0-2 hours) in each stream.

3.4 Energy budget

Attempts to determine reach-scale aquifer-stream exchange from the temperature dynamics in each stream using the HFLUX Stream Temperature Solver (Glose et al., 2017) were unsuccessful. Although the model captured the diel temperature signal in each stream, it failed to accurately estimate the observed increases and decreases in temperature with distance downstream in GC and BB, respectively. This necessitated the creation of a site specific energy budget for determination of the dominant energy fluxes over the study reaches within the stream systems (Figures 3.20 and 3.21). Net shortwave radiation was the primary mechanism of energy gain, while latent heat exchange was the dominant process by which heat was lost in each stream over the study period. Both latent and sensible heat were of similar magnitude, but opposite direction, while bed conduction was negligible. Although the individual components of

longwave radiation were of notable magnitude, net longwave radiation was negligible. Frictional heating from the streambed was excluded due to the formulation of Theurer et al. (1984) yielding values of unreasonable magnitude compared to other calculated fluxes. With the omission of frictional heating, average net energy gain to GC and BB over the period of June 22 to September 5, 2016 was 7.99 MJ/m^2 Day (93.37 W/m^2) and 9.45 MJ/m^2 Day (110.40 W/m^2), respectively (Table 3.1). This indicated that stream temperature increased with distance downstream. Although this is generally expected behaviour of stream temperature, it is contrary to the cooling observed in BB.

Chapter 4: Discussion

The thermal regime of a stream is described as the observed spatiotemporal patterns in variations of water temperature (Caissie, 2006). Alpine stream thermal regimes are exceptionally important as they often allow for establishment of thermal and climatic refugia for cold-water fish species (Dugdale et al., 2013; Harrington, 2017; Isaak et al., 2015). Stream temperature is thus a major subject of research globally due to its importance to in-stream biogeochemical conditions and susceptibility to climate change (Brown and Hannah, 2008; Kelleher et al., 2012). The understanding of the fundamental processes controlling water temperature and variability in headwater streams is limited (Khamis et al., 2015), primarily due to the complex spatiotemporal variations of energy fluxes contributing towards the thermal regimes (Kelleher et al., 2012). However, the body of literature highlighting the distinct characteristics of thermal regimes and heat exchange in alpine streams is growing (e.g., Khamis et al., 2015; Leach and Moore, 2017; Webb et al., 2008). With the risk that future warming due to climate change holds to thawing permafrost (Okkonen et al., 2010), study of rivers in permafrost regions has increased, but those that focus on stream temperature dynamics typically involve much larger, more accessible river

systems (e.g., King et al., 2016; Yang et al., 2014). Thus, a knowledge gap exists regarding the thermal dynamics of permafrost underlain alpine basins.

The purpose of this study is to determine the distinct characteristics of the thermal regimes and the dominant heat fluxes within alpine streams in permafrost catchments. Specific objectives are to (1) identify and describe the spatiotemporal thermal patterns in two alpine streams underlain by discontinuous permafrost, and (2) quantify the dominant energy fluxes contributing to these patterns through an energy budget approach. The motivation behind this is that although water temperature and variability in headwater streams has important ecological and biogeochemical implications in a changing climate (Caissie, 2006; Gooseff, 2010), understanding of the processes controlling these thermal regimes is limited (Khamis et al., 2015). The thermal regimes of alpine streams are of further importance for the study of climate change as their low temperatures commonly offer thermal and climatic refugia for cold water aquatic species (Dugdale et al., 2013; Harrington, 2017; Isaak et al., 2015).

4.1 Spatiotemporal trends and implications

4.1.1 Spatial cooling, response to tributaries, and groundwater influence

Observed mean diel thermal amplitudes (1.5˚C and 1˚C in GC and BB, respectively) and mean water temperatures (5.9˚C and 6.1˚C in GC and BB, respectively) are much lower than temperate systems. For example, in Catamaran Brook, New Brunswick, typical mean diel thermal amplitudes and water temperatures are 3˚C and 10˚C, respectively (Caissie and Luce, 2017). By comparison, these values are also lower than that observed in the glacial fed Taillon-Gabriétous catchment, Cirque de Governie, French Pyrénées with mean thermal amplitudes and water temperatures of 6.3˚C and 7.8˚C, respectively (Khamis et al., 2015). Although each stream has common characteristics, they exhibit notable heterogeneity in spatial trends. Plots of longitudinal water temperature highlighted areas of consistent temperature decrease, as well as a

distinct response to tributary inflow in each stream (Figures 3.5b and 3.6). Based on the cooling influence that upwelling groundwater can have locally in small streams (Poole et al., 2008), locations exhibiting consistent temperature decrease along each stream are likely a result of a groundwater influence.

Neither stream warms appreciably with distance downstream, with BB showing an average overall cooling pattern (Figures 3.6 and 3.7). This is likely due to downstream shading blocking incident solar radiation (Figures 2.2a and 2.6) combined with the influence of groundwater within each catchment. Further, steep streambed gradients over the study reaches may contribute to marginal warming as high slopes result in lower warming of water temperatures with distance downstream by lowering residence times for water to gain heat from its surroundings (Mayer, 2012; Webb et al., 2008). The primary tributary to GC flows from a wetland complex on the south-facing slope and is therefore much warmer, accounting for the observed warming effect it has at 1150 m downstream. Conversely, as the tributary to BB has no identifiable headwaters and exerts a strong cooling effect at their confluence (1600 m downstream), it is assumed that this is groundwater sourced (Figure 3.6). This is supported by the observation that groundwater contributes to streamflow of creeks in the WCRB alpine regions (Seguin et al., 1999), as well as the sharp decrease (increase) in mean air-water temperature linear regression slope (intercept) at 1600 m downstream (Figure 3.11).

The inference of groundwater upwelling occurring at the locations of consistent temperature decrease in each stream is further supported by patterns in longitudinal SpC (Figures 3.8 and 3.9). Increases in SpC along each stream are seen to occur coincidentally with identified locations of temperature decrease. As in temperate environments, the chemistry of groundwater in permafrost regions is largely dependent on flow path (residence time) and aquifer mineral

assemblage, resulting in distinct chemical compositions. In shallow (suprapermafrost) systems, groundwater is often reflective of snowmelt and precipitation with high organic content, whereas water in deep (intra and sub-permafrost) systems is typically more saline (van Everdingen et al., 1990). Further, in areas with decreased permafrost, soil water is able to infiltrate much deeper, resulting in longer residence times and increased mineralization, producing considerably older water with a higher electrical conductivity entering the stream along these flowpaths (Hinzman et al., 2005). Thus, these increases in SpC are indicative of a possible groundwater source contributing to local cool spots along each stream. Decrease of SpC upon tributary inflow to BB suggests that the source to this tributary is a different, shallower aquifer from that of upwelling groundwater contributing to other areas of local cooling along its length.

As BB exhibits more downstream heterogeneity in its thermal regime than GC, a stronger influence of groundwater over its study reach is assumed. This is supported by observed overall downstream cooling (Figure 3.7) with more locations of temperature decrease along its study reach (Figure 3.6) and patterns seen in regression slope and intercept, seasonal streamflow, and spatiotemporal temperature variance. Linear regression between mean daily air and water temperature is often used in investigations of groundwater influence and thermal sensitivity in streams (Caissie, 2006; Kelleher et al., 2012; Mayer, 2012). As discussed, the regression slope and intercept of groundwater dominated streams will be lower and higher, respectively than that of non-groundwater dominated catchments (Caissie, 2006) due to the damping effect that upwelling groundwater can have on stream temperature change (Poole et al., 2008). Regression slope also provides a first order approximation of the thermal sensitivity of a stream to air temperature change (high/low slope shows high/low sensitivity), and is important for

understanding and predicting future impacts due to climate change (Kelleher et al., 2012; Mayer, 2012).

The patterns identified in mean daily air and water temperature regression slope and intercept indicate that each stream experiences an increasing groundwater influence (Caissie, 2006) and decreasing thermal sensitivity (Kelleher et al., 2012; Mayer, 2012) with distance downstream. These also highlight the presence of focused upwelling at various locations in the upper study reaches of each stream (Caissie, 2006), supporting observations of local cooling (Figures 3.6, 3.10, and 3.11). The common mean regression slope (0.37) shared by the streams reflects an equal thermal sensitivity over their study reaches. However, BB having a higher mean regression intercept (2.1˚C) than GC (1.2˚C) indicates a stronger influence of groundwater. This is further highlighted with BB having consistently lower regression slopes and higher intercepts with distance downstream than GC. Comparison of streamflow timing in GC and BB further demonstrates a stronger groundwater influence in BB. Greater freshet discharge in GC is evidence of more suprapermafrost flows due to increased underlying permafrost and thus a smaller influence of groundwater. Further, augmented discharge in BB over the majority of the post-freshet observation period (July 12 onward) indicates a higher baseflow and consequently a larger groundwater influence (Figure 3.3a). This conclusion is strengthened by the observed behaviour in spatial variance of temperature in each stream. Each creek displays decreasing variance with distance downstream, with locations of sudden decrease coinciding with that of consistent temperature decreases as well as decreases (increases) of regression slope (intercept) (Figures 3.6, 3.10, 3.11, and 3.12a). The higher temporal variance in GC is also an indication of its higher thermal sensitivity and thus a possible lower influence of groundwater when compared to BB (Figure 3.12b).

An important consideration for this study is that thermal sensitivity in small streams varies as a result of multiple, interacting controls. As both groundwater sourced and shaded streams exhibit lower thermal sensitivities (Kelleher et al., 2012), it is difficult to differentiate between the relative controls of increasing groundwater influence and shading with distance downstream in these catchments. Although shading is likely a contributing factor to the above patterns, channel shading in each stream is relatively similar with distance downstream (Figure 2.6), and thus groundwater is likely the dominant control on their thermal regimes.

4.1.2 Stream thermal response

The observed thermal response of each stream to incoming shortwave radiation shows a strong synchroneity between stations along the length of each. These observations reinforce those made by Brown and Hannah (2008), rather than a pulse of warmer water moving downstream, resulting in successive stations downstream registering maximums at later times than those upstream. Although the maximums occurred synchronously, which could indicate higher thermal sensitivity, the large range in water temperature maximums among sites is contradictive to that, signaling a strong thermal heterogeneity within each stream (Figure 3.13). The observation of water temperatures often reaching their daily maximum prior to air temperature (negative lag, Figures 3.14 and 3.15) is as yet unreported in the literature. However, it is hypothesized that this occurs as a combination of shallow water depths and coarse bed material, coupled with long, sunny days. Shallow water depths (mean depth: 0.26 m and 0.24 m in GC and BB, respectively) along each creek allow the streambed to gain more heat during these long days with considerable solar input. As the predominant bed material is composed of very coarse gravels, cobbles, and boulders, the streambed has a relatively low heat capacity and higher effective thermal conductivity (based on the general relation between thermal conductivity (K) of saturated sediments and their dry-bulk densities (ρ_b), K of 0.8 W/m˚C to 2.5

W/m˚C for ρ_b of 1.2 g/cm^3 to 1.8 g/cm^3, respectively; Lapham, 1989) compared to that of water. This could allow for more efficient storage of heat gained by the streambed material, radiating it back into the water column overnight and into the early morning. This release of heat could act to buffer the overnight decrease in water temperature, where it then continues heating upon receiving insolation, thus peaking sooner than that of the air on subsequent days. This is strengthened by the observation that overnight minimum streambed temperature at vertical temperature profile locations is often higher than that of minimum water temperature (0.1˚C – 0.2˚C), indicating heat conduction into the water column. Contrasting lags in air-water temperature (negative) and net radiation-water temperature (positive) occur more often on days with decreased cloud cover. Comparatively, concurrent negative lags in air-water temperature and net radiation-water temperature arise on days with increased cloud cover and occur much less frequently (Figures 3.17 and 3.18).

4.1.3 Vertical temperature behaviour and downwelling

Inferred downwelling at the locations of vertical streambed temperature profiles in each stream is based on observed efficient downward propagation of the diel temperature signal into the streambed sediment (Figure 3.19a). High coefficient of determination values (0.996-1) and low lag times (0-2 hours) determined through cross-correlation of water and streambed sediment temperature support these observations. These short lags in each stream are also consistent with the range observed in downwelling zones in a headwater stream by Moore et al. (2005). Analysis with VFLUX 2 (Gordon et al., 2012; Irvine et al., 2015) was unable to calculate associated flux values of downwelling water at any of the sites. This likely occurred due to sensors being too closely spaced combined with strong downwelling, resulting in a minimal temperature gradient with depth and the amplitude ratio of the temperature signals being equal to or greater than one for much of the time-series (Gordon et al., 2012). Although the amplitude ratios being near one

is indicative of strong downwelling occurring (no shift or lag in the diel signal with depth), the developed methods require a difference in amplitudes in order to calculate flux (Gordon et al., 2012). Pronounced downwelling at vertical streambed profile locations within each stream combined with inferred upwelling suggests the presence of groundwater cycling and high rates of hyporheic exchange within each stream.

4.2 Energy budget and implications

4.2.1 Applicability of HFLUX

As noted in Chapter 3, the failure of HFLUX (Glose et al., 2017) to accurately estimate the increases and decreases in temperature with distance downstream in each stream resulted in the inability to determine reach-scale aquifer-stream exchange. Failure of the model is credited to insufficient downstream change in discharge in the upper study reaches of each stream. Longitudinal plots of mean downstream discharge show this, with an increase of less than 10 % between the top three discharge stations in BB, and a losing section (25.8 % decrease in flow) in the uppermost study reach of GC (Figure 3.3b). This flow behaviour is due to groundwater cycling and high rates of hyporheic exchange within each stream, as suggested by the combination of pronounced downwelling at vertical temperature profile locations and inferred upwelling at various locations along each. The failure of HFLUX facilitated the creation of an energy budget for evaluation of the dominant energy fluxes in each system.

4.2.2 Energy fluxes

4.2.2.1 Energy budget uncertainty

Determination of most distributed energy fluxes in streams has an amount of associated uncertainty. The accuracy of measuring instruments, small range of assumed parameters (emissivity and albedo), and small correction factors (view-to-sky and shading factor) make for accurate approximation of radiative fluxes. However, the use of standard empirical equations for calculation of longwave radiation emitted by the stream surface and landcover introduces

uncertainty (Leach and Moore, 2010). This is large in the calculation of longwave radiation emitted by landcover due to the assumption that temperature of the canopy is equal to air temperature. Compared to radiative fluxes, turbulent fluxes have larger associated uncertainties due to their driving meteorological data being measured on an adjacent plateau of higher elevation and considerably shorter vegetation. Thus, it is assumed that both windspeed and vapour pressure are lower and higher, respectively at the stream surface than on the plateau. These differences result in the possibility of latent heat flux being overestimated and the magnitude of the Bowen ratio being underestimated, thus either overestimating or underestimating sensible heat flux. Perhaps more importantly, equations used to determine turbulent fluxes are perhaps not appropriate for small width streams due to the underlying boundary-layer assumptions in the application of Equations 9 – 16. Regardless of this, these equations are used broadly in stream temperature research to estimate turbulent fluxes from the stream. Uncertainty in streambed conductive heat flux is due to the assumed constant streambed temperature and effective thermal conductivity throughout the study reaches. Finally, the use of Theurer et al.'s (1984) formulation to determine frictional heating introduces a large uncertainty due to the aforementioned assumption that all gravitational potential is converted into frictional heating.

Validity of the energy budget can be evaluated through comparison of estimated and observed temperature change between the 'upstream' and 'outlet' locations. Average net energy gain from distributed energy fluxes (omitting frictional heating) over the study reaches during the June 22 to September 5 study period was 7.99 MJ/m^2Day (93.37 W/m^2) and 9.45 MJ/m^2Day (110.40 W/m^2) in GC and BB, respectively (Table 3.1). Approximated average rate of

temperature change due to distributed energy fluxes along each stream ($\frac{\partial T}{\partial x}$, ˚C/m) was calculated using (Harrington, 2017):

$$\frac{\partial T}{\partial x} = \frac{q_n * w}{Q * C_w} \tag{20}$$

where q_n is the net distributed energy flux (W/m^2), w is mean channel width along the reach (m), Q is mean discharge along the reach (m^3/s), and C_w is the volumetric heat capacity of water (set at a constant of 4.18×10^6 J/m^{3}K). Assuming mean widths of 2.32 m (GC) and 1.93 m (BB), and average stream discharge of 0.13 m^3/s, approximated average temperature increase over the study period is 0.8˚C along the 1950 m reach of each stream. For GC, this is in agreement with the observed average temperature difference of 0.9˚C between the 'upstream' and 'outlet' locations. However, it is lower than that computed with the slope of the linear fit line to the mean study period longitudinal stream temperatures (1.3˚C). In BB, the approximated average temperature increase does not agree with the observed average temperature difference of -0.1˚C between the 'upstream' and 'outlet' locations. It also does not correspond with the temperature decrease determined from the slope of the linear fit line to the mean longitudinal stream temperatures (-0.4˚C). Including frictional heating results in an average temperature increase of 1.1˚C along the 1950 m reach in GC, indicating that although there are uncertainties in the calculation of the turbulent, bed, and frictional energy fluxes, the energy budget is plausible. Conversely, including frictional heating in BB results in an average temperature increase of 1.2˚C along the 1950 m reach, indicating the likelihood of a large unaccounted for energy sink within the system. This highlights the potential of a source of groundwater contributing to cooling along the reach of BB. Further, neglecting the energy fluxes from tributaries to each stream results in a large uncertainty in each energy budget. The ability to include energy fluxes

from tributaries would result in more accurate estimations of temperature change and groundwater influence over the study reaches.

With the above mentioned uncertainties, calculated flux values still compare reasonably well with the literature. However, each study has considerable differences in reach length, vegetation, and study period length. For example Harrington (2017) reported a net energy gain from distributed energy fluxes of 9.2 MJ/m^{2}Day (107 W/m^2) for a July – August 2016 study period in Helen Creek, Alberta. This catchment showed considerably differing magnitudes in fluxes of shortwave radiation (17.7 MJ/m^{2}Day), longwave radiation (-4.4 MJ/m^{2}Day), latent heat (-5.1 MJ/m^{2}Day), sensible heat (-0.2 MJ/m^{2}Day), and bed conduction (1.8 MJ/m^{2}Day) than calculated for GC and BB (Table 3.1). This study reach of Helen Creek however, is only 545 m long, considerably higher elevation (2225 m – 2374 m) and lower gradient (1.7%), partially glacial fed, and un-vegetated. This differing character accounts for the greater flux magnitudes, as well as the differences in losses and gains from respective fluxes compared to GC and BB. Although the flux values between the catchments are distinct, the key driving fluxes of shortwave radiation and latent heat for energy gain and loss, respectively are still present.

4.2.2.2 Controls to stream temperature

Although uncertainties in the energy budget make determination of controlling fluxes difficult, interpretations can still be made. The dominance of shortwave radiation and latent heat flux for respective heat gain and loss is common during the summer season in alpine streams (e.g., Khamis et al., 2015; Magnusson et al., 2012; Somers et al., 2016). In GC, it is likely that shortwave radiation is responsible in controlling the increases in temperature over its upper reach (0 m to 1100 m downstream, Figure 3.6). Temperature increases observed in the lower reach of GC are then due to the inflow of tributaries at 1150 m and 1450 m downstream, combined with increased longwave radiation gained from increasing density of riparian vegetation. The overall

low rate of temperature increase seen in GC is likely due to the combination of groundwater, shading, and steep gradient suggested earlier. Again, shortwave radiation is likely the cause of temperature peaks observed in the upper reach (0 m to 1100 m downstream, Figure 3.6) of BB. However, the downstream cooling observed in BB makes it much more difficult to generalize, as the loss of heat due to latent heat exchange is not great enough to account for this. Thus, this overall downstream cooling trend is likely due primarily to the influence of groundwater over the study reach, strengthening inferences made from observations discussed previously.

Through use of a simple advective heat balance, the groundwater discharge required to account for the minimal increase in temperature in GC and the overall cooling in BB can be estimated:

$$Q_u T_u + Q_{gw} T_{gw} = Q_o T_o \quad (21)$$

where Q represents mean discharge (m^3/s), T represents mean water temperature (˚C), and the subscripts u, gw, and o represent upstream boundary, groundwater, and outlet sampling, respectively. Assuming Q_u of 0.12 m^3/s (GC) and 0.06 m^3/s (BB), T_u of 5.3˚C (GC) and 6.1˚C (BB), T_o of 6.3˚C (GC) and 6.0˚C (BB), Q_o of 0.13 m^3/s, and T_{gw} (mean temperature in shallow riparian wells) of 3.1˚C (GC) and 5.8˚C (BB), approximated mean groundwater inflow over the study period is 0.06 m^3/s (GC) and 0.07 m^3/s (BB). Assuming mean widths used in Equation (20) results in mean upwelling rates of 1.3×10^{-5} m/s and 1.9×10^{-5} m/s over the 1950 m reach of GC and BB, respectively. Over the 76-day (6566400 s) observation period, these calculated rates produce sizable volumes and depths of water flowing into the study reaches of GC (3.9×10^5 m^3 and 8.7×10^4 mm) and BB (4.6×10^5 m^3 and 1.2×10^5 mm). Although there is much uncertainty involved in these estimations, upwelling rates are of similar magnitude to those seen in the literature (Burkholder et al., 2008; Gordon et al., 2012). These approximations of potential

groundwater flux to each stream further strengthen the inferences made of the increased influence of groundwater over the study reach of BB.

Without further collection of field data, there is a challenge in determining the overarching role that permafrost plays in the thermal regime of each stream. However, its presence is likely indirectly related to the observed patterns in spatiotemporal cooling, low mean diel thermal amplitudes (GC: 1.5˚C, BB: 1˚C), and low mean water temperatures (GC: 5.9˚C, BB: 6.1˚C) discussed previously. Although the above mentioned patterns are assumed to be the result of a strong groundwater influence over the study reach of each stream, the magnitude of its effect is likely due to the presence of permafrost resulting in significantly cooler water upwelling within each stream. This results in a greater buffering of diel thermal amplitudes and lower mean water temperatures than might be observed in each stream with the absence of permafrost. Further, the distribution of permafrost could also play a part in determining the spatial distribution of inferred zones of upwelling by restricting groundwater flow through parts of the study reaches (Prowse et al., 1990). An additional challenge to investigations in alpine permafrost catchments such as the WCRB is accessibility. Rugged terrain and limited means of entry result in high costs associated with characterizing groundwater and permafrost in these regions, and doing so is often less appealing unless associated with economic benefits.

Chapter 5: Summary and Conclusions

The existing knowledge gap of the fundamental controls to thermal dynamics of headwater streams in permafrost catchments creates an important opportunity for further research. This is not only due to the strong sensitivity of both permafrost and stream temperatures to climate warming (e.g., Arora et al., 2016; Okkonen et al., 2010), but also the likelihood of permafrost playing an important role in the overall contribution towards stream

temperature and variability in these regions. This study analyzes the patterns of thermal regimes and energy fluxes in two discontinuous permafrost underlain alpine streams in the Yukon Territory. The aim of this research was to determine the distinctive characteristics of alpine stream thermal regimes and the influence of respective heat fluxes on observed water temperature patterns.

Although the overall study period was short, the high density and frequency of monitoring revealed important thermal processes and unique spatiotemporal trends. Key findings from this study are:

1) Distinct thermal heterogeneity in each stream indicates areas of focused groundwater upwelling and an increasing groundwater influence with distance downstream. Focused upwelling is inferred from locations along the length of each stream displaying persistent temperature decrease that are coincident with increases in SpC and trends of mean air-water temperature linear regression slope and intercept. Increasing downstream groundwater influence is supported by increasing (decreasing) mean air-water linear regression intercepts (slopes) with distance downstream, and an overall decrease in stream temperature with distance downstream in BB and a minimal increase in temperature with distance downstream in GC. Lower (higher) values of regression slope (intercept) with distance downstream and greater baseflow in BB indicate a stronger groundwater influence over its study reach.
2) Overall low thermal sensitivity of each stream and decreasing sensitivity with distance downstream, indicated by the low mean air-water temperature regression slope shared by the streams (0.37) and values that decrease with distance in each stream. The lower values of regression slope with distance downstream in BB indicate a lower thermal

sensitivity over its study reach than that of GC. This indicates that the upper study reaches of each stream are more susceptible to future increases in air temperature than that of the lower reaches.

3) Observed negative lags between maximums of air and water temperature, and net radiation and water temperature in each stream are as yet unreported in the literature. This phenomenon is seen in plots of diel air and water temperature, and diel net radiation and water temperature, with the frequent occurrence of daily stream temperature along the length of each stream peaking prior to that of air temperature during extended periods of warm weather (increased insolation). Contrasting lags in air-water temperature (negative) and net radiation-water temperature (positive) are typically observed on days with less cloud cover. Conversely, concurrent negative lags in air-water temperature and net radiation-water temperature occur on days with increased cloud cover and occur much less frequently.
4) The presence of strong downwelling within each stream, indicating hyporheic exchange and groundwater cycling. This is seen in efficient downward propagation of the diel temperature signal into the streambed at locations of vertical temperature profiles and is supported by various locations of inferred upwelling along the study reaches.

These findings highlight the importance of continued study of thermal regimes and the complicated interconnections between heat exchange processes in alpine catchments in permafrost regions. Further research is required to evaluate whether: 1) observations made over one summer season of study are accurate representations of the thermal regimes of GC and BB, and 2) if these two basins are illustrative of other permafrost underlain alpine watersheds.

References

Arora, R., Tockner, K., Venohr, M., 2016. Changing river temperatures in northern Germany: Trends and drivers of change. Hydrol. Process. 30, 3084–3096. doi:10.1002/hyp.10849

Boano, F., Harvey, J.W., Marion, A., Packman, A.I., Revelli, R., Ridolfi, L., Wörman, A., 2014. Hyporheic flow and transport processes: Mechanisms, models, and bioghemical implications. Rev. Geophys. 52, 1–77. doi:10.1002/2012RG000417.Received

Boyd, M., Kasper, B., 2003. Analytical Methods for Dynamic Open Channel Heat and Mass Transfer: Methodology for the Heat Source Model Version 7.0 204.

Brown, L.E., Hannah, D.M., 2008. Spatial heterogeneity of water temperature across an alpine river basin. Hydrol. Process. 22, 954–967. doi:10.1002/hyp.6982

Brown, R.J.E., 1970. Permafrost in Canada: Its influence on northern development. University of Toronto Press.

Brown, R.J.E., Kupsch, W.., 1974. Permafrost Terminology.

Burkholder, B.K., Grant, G.E., Haggerty, R., Khangaonkar, T., Wampler, P.J., 2008. Influence of hyporheic flow and geomorphology on temperature of a large, gravel-bed river, Clackamas River, Oregon, USA. Hydrol. Process. 22, 941–953. doi:10.1002/hyp.6984

Caissie, D., 2006. The thermal regime of rivers: A review. Freshw. Biol. 51, 1389–1406. doi:10.1111/j.1365-2427.2006.01597.x

Caissie, D., Luce, C.H., 2017. Quantifying streambed advection and conduction heat fluxes Daniel. Water Resour. Res. 53, 1595–1624. doi:10.1002/2016WR019813

Carey, S.K., Boucher, J.L., Duarte, C.M., 2013. Inferring groundwater contributions and pathways to streamflow during snowmelt over multiple years in a discontinuous permafrost subarctic environment (Yukon, Canada). Hydrogeol. J. 21, 67–77. doi:10.1007/s10040-012-0920-9

Carey, S.K., Quinton, W.L., 2005. Evaluating runoff generation during summer using hydrometric , stable isotope and hydrochemical methods in a discontinuous permafrost alpine catchment. Hydrol. Process. 19, 95–115. doi:10.1002/hyp.5764

DeBeer, C.M., Wheater, H.S., Carey, S.K., Chun, K.P., 2016. Recent climatic, cryospheric, and hydrological changes over the interior of western Canada: A review and synthesis. Hydrol. Earth Syst. Sci. 20, 1573–1598. doi:10.5194/hess-20-1573-2016

Dingman, S.L., 2002. Physical Hydrology. Prentice-Hall, Upper Sadle River, New Jersey.

Dugdale, S.J., Bergeron, N.E., St-hilaire, A., 2013. Temporal variability of thermal refuges and water temperature patterns in an Atlantic salmon river. Remote Sens. Environ. 136, 358–373. doi:10.1016/j.rse.2013.05.018

Environment and Climate Change Canada, 2017. Canadian Climate Normals, 1981-2010 Station Data [WWW Document]. URL http://climate.weather.gc.ca/climate_normals/results_1981_2010_e.html?searchType=stnName&txtStationName=Whitehorse&searchMethod=contains&txtCentralLatMin=0&txtCentralLatSec=0&txtCentralLongMin=0&txtCentralLongSec=0&stnID=1617&dispBack=0 (accessed 6.28.17).

Environment and Climate Change Canada, 2013. Rivers [WWW Document]. URL https://www.ec.gc.ca/eau-water/default.asp?lang=En&n=45BBB7B8-1#canada (accessed 7.5.17).

Evans, E.C., Petts, G.E., 1997. Hyporheic temperature patterns within riffles. Hydrol. Sci. J. 42, 199–213. doi:10.1080/02626669709492020

Ge, S., McKenzie, J., Voss, C., Wu, Q., 2011. Exchange of groundwater and surface - water mediated by permafrost response to seasonal and long term air temperature variation. Geophys. Res. Lett. 38, 1–6. doi:10.1029/2011GL047911

Glose, A.M., Lautz, L.K., Baker, E.A., 2017. Stream heat budget modeling with HFLUX: Model development, evaluation, and applications across contrasting sites and seasons. Environ. Model. Softw. 92, 213–228. doi:10.1016/j.envsoft.2017.02.021

Gooseff, M.N., 2010. Defining hyporheic zones - advancing our conceptual and operational definitions of where stream water and groundwater meet. Geogr. Compass 4, 945–955. doi:10.1111/j.1749-8198.2010.00364.x

Gordon, R.P., Lautz, L.K., Briggs, M.A., McKenzie, J.M., 2012. Automated calculation of vertical pore-water flux from field temperature time series using the VFLUX method and computer program. J. Hydrol. 420–421, 142–158. doi:10.1016/j.jhydrol.2011.11.053

Hannah, D.M., Malcolm, I.A., Soulsby, C., Youngson, A.F., 2008. A comparison of forest and moorland stream microclimate, heat exchanges and thermal dynamics. Hydrol. Process. 22, 919–940. doi:10.1002/hyp.7003

Hari, R.E., Livingstone, D.M., Siber, R., Burkhardt-Holm, P., Guttinger, H., 2006. Consequences of climatic change for water temperature and brown trout populations in Alpine rivers and streams. Glob. Chang. Biol. 12, 10–26. doi:10.1111/j.1365-2486.2005.01051.x

Harrington, J.S., 2017. The Hydrogeology of a Rock Glacier and Its Effect on Stream Temperature. University of Calgary.

Hinzman, L.D., Kane, D.L., Woo, M., 2005. Permafrost Hydrology. Encycl. Hydrol. Sci. 14, 1–15. doi:10.1002/0470848944

Irvine, D.J., Briggs, M.A., Lautz, L.K., Gordon, R.P., McKenzie, J.M., Cartwright, I., 2017. Using Diurnal Temperature Signals to Infer Vertical Groundwater-Surface Water Exchange. Groundwater 55, 10–26. doi:10.1111/gwat.12459

Irvine, D.J., Lautz, L.K., Briggs, M.A., Gordon, R.P., McKenzie, J.M., 2015. Experimental evaluation of the applicability of phase, amplitude, and combined methods to determine water flux and thermal diffusivity from temperature time series using VFLUX 2. J. Hydrol. 531, 728–737. doi:10.1016/j.jhydrol.2015.10.054

Isaak, D.J., Young, M.K., Nagel, D.E., Horan, D.L., Groce, M.C., 2015. The cold-water climate shield: Delineating refugia for preserving salmonid fishes through the 21st century. Glob. Chang. Biol. 21, 2540–2553. doi:10.1111/gcb.12879

Kelleher, C., Wagener, T., Gooseff, M., Mcglynn, B., Mcguire, K., Marshall, L., 2012. Investigating controls on the thermal sensitivity of Pennsylvania streams. Hydrol. Process. 26, 771–785. doi:10.1002/hyp.8186

Khamis, K., Brown, L.E., Milner, A.M., Hannah, D.M., 2015. Heat exchange processes and thermal dynamics of a glacier-fed alpine stream. Hydrol. Process. 29, 3306–3317. doi:10.1002/hyp.10433

King, T. V., Neilson, B.T., Overbeck, L.D., Kane, D.L., 2016. Water temperature controls in low arctic rivers Tyler. Water Resour. Res. 52, 4358–4376. doi:10.1002/2015WR017965

Kurylyk, B.L., Moore, R.D., Macquarrie, K.T.B., 2016. Scientific briefing: Quantifying streambed heat advection associated with groundwater-surface water interactions. Hydrol. Process. 30, 987–992. doi:10.1002/hyp.10709

Lapham, W.W., 1989. Use of temperature profiles beneath streams to determine rates of vertical ground-water flow and vertical hydraulic conductivity. US Geol. Surv. Water-Supply Pap. 2337 35. doi:Cited By (since 1996) 47\nExport Date 4 April 2012

Leach, J.A., Moore, R.D., 2017. Insights on stream temperature processes through development of a coupled hydrologic and stream temperature model for forested coastal headwater catchments. Hydrol. Process. doi:10.1002/hyp.11190

Leach, J.A., Moore, R.D., 2014. Winter stream temperature in the rain-on-snow zone of the Pacific Northwest: Influences of hillslope runoff and transient snow cover. Hydrol. Earth Syst. Sci. 18, 819–838. doi:10.5194/hess-18-819-2014

Leach, J.A., Moore, R.D., 2010. Above-stream microclimate and stream surface energy exchanges in a wildfire-disturbed riparian zone. Hydrol. Process. 24, 2369–2381. doi:10.1002/hyp.7639

Lisi, P.J., Schindler, D.E., Cline, T.J., Scheuerell, M.D., Walsh, P.B., 2015. Watershed geomorphology and snowmelt control stream thermal sensitivity to air temperature. Geophys. Res. Lett. 42, 3380–3388. doi:10.1002/2015GL064083.Received

Maclean, R., Oswood, M.W., Irons III, J.G., Mcdowell, W.H., 1999. The Effect of Permafrost on Stream Biogeochemistry : A Case Study of Two Streams in the Alaskan (U.S.A.) Taiga. Biogeochemistry 47, 239–267.

Magnusson, J., Jonas, T., Kirchner, J.W., 2012. Temperature dynamics of a proglacial stream: Identifying dominant energy balance components and inferring spatially integrated hydraulic geometry. Water Resour. Res. 48, 1–16. doi:10.1029/2011WR011378

Malard, F., Tockner, K., Dole-Olivier, M.-J., Ward, J. V, 2002. A landscape perspective of surface – subsurface hydrological exchanges in river corridors. Freshw. Biol. 47, 621–640.

Marsh, P., Prowse, T.D., Ommanney, C., 1990. Snow hydrology. In: Northern Hydrology: Canadian Perspectives.

Mayer, T.D., 2012. Controls of summer stream temperature in the Pacific Northwest. J. Hydrol. 475, 323–335. doi:10.1016/j.jhydrol.2012.10.012

McCartney, S.E., Carey, S.K., Pomeroy, J.W., 2006. Intra-basin variability of snowmelt water balance calculations in a subarctic catchment. Hydrol. Process. 20, 1001–1016. doi:10.1002/hyp.6125

Moore, R.D., Sutherland, P., Gomi, T., Dhakal, A., 2005. Thermal regime of a headwater stream within a clear-cut , coastal British Columbia , Canada. Hydrol. Process. 19, 2591–2608. doi:10.1002/hyp.5733

Okkonen, J., Jyrkama, M., Kløve, B., 2010. A conceptual approach for assessing the impact of climate change on groundwater and related surface waters in cold regions (Finland). Hydrogeol. J. 18, 429–439. doi:10.1007/s10040-009-0529-9

Pepin, N., Bradley, R.S., Diaz, H.F., Baraer, M., Caceres, E.B., Forsythe, N., Fowler, H., Greenwood, G., Hashmi, M.Z., Liu, X.D., Miller, J.R., Ning, L., Ohmura, A., Palazzi, E., Rangwala, I., Schöner, W., Severskiy, I., Shahgedanova, M., Wang, M.B., Williamson, S.N., Yang, D.Q., 2015. Elevation-dependent warming in mountain regions of the world. Nat. Clim. Chang. 5, 424–430. doi:10.1038/nclimate2563

Pomeroy, J., Hedstrom, N., Parviainen, J., 1999. The Snow Mass Balance of Wolf Creek , Yukon : Effects of Snow Sublimation and Redistribution, in: Pomeroy, J.W., Granger, R. (Eds.), Wolf Creek Research Basin: Hydrology, Ecology, Environment. Environment Canada: Saskatoon, pp. 15–30.

Poole, G.C., O'Daniel, S.J., Jones, K.L., Woessner, W.W., Bernhardt, E.S., Helton, A.M., Stanford, J.A., Boer, B.R., Beechie, T.J., 2008. Hydrologic Spiralling : The Role of Multiple Interactive Flow Paths in Stream Ecosystems. River Res. Appl. 24, 1018–1031. doi:10.1002/rra.1099

Prowse, T.D., Ommanney, C., Simon, L., 1990. Northern hydrology: An overview. In: Northern Hydrology: Canadian Perspectives.

Rasmus, S., Gustafsson, D., Koivusalo, H., Laurén, A., Grelle, A., Kauppinen, O.K., Lagnvall, O., Lindroth, A., Rasmus, K., Svensson, M., Weslien, P., 2013. Estimation of winter leaf area index and sky view fraction for snow modelling in boreal coniferous forests: Consequences on snow mass and energy balance. Hydrol. Process. 27, 2876–2891. doi:10.1002/hyp.9432

Schwab, M., Klaus, J., Pfister, L., Weiler, M., 2016. Diel discharge cycles explained through viscosity fluctuations in riparian inflow. Water Resour. Res. 52, 8744–8755. doi:10.1002/2016WR018626

Seguin, M.-K., Stein, J., Nilo, O., Jalbert, C., Ding, Y., 1999. Hydrogeophysical Investigation of the Wolf Creek Watershed, Yukon Territory, Canada. Proc. from Wolf Creek Res. Basin Hydrol. Ecol. Environ. Work. Whitehorse, Yukon 55–78.

Somers, L.D., Gordon, R.P., McKenzie, J.M., Lautz, L.K., Wigmore, O., Glose, A.M., Glas, R., Aubry-Wake, C., Mark, B., Baraer, M., Condom, T., 2016. Quantifying groundwater-surface water interactions in a proglacial valley, Cordillera Blanca, Peru. Hydrol. Process. 30, 2915–2929. doi:10.1002/hyp.10912

The Mathworks Inc., 2016. MATLAB Version 9.1.0.

Theurer, F.D., Voos, K.A., Miller, W.J., 1984. Instream water temperature model. Instream Flow Inf. Pap. 16.

van Everdingen, R.O., Prowse, T.D., Ommanney, C., 1990. Ground-water hydrology. In: Northern Hydrology: Canadian Persepctives.

Walvoord, M.A., Kurylyk, B.L., 2016. Hydrologic impacts of thawing permafrost - a review. Vadose Zo. J. 15, 1–20. doi:10.2136/vzj2016.01.0010

Webb, B.W., Hannah, D.M., Moore, R.D., Brown, L.E., Nobilis, F., 2008. Recent advances in stream and river temperature research. Hydrol. Process. 22, 902–918. doi:10.1002/hyp.6994

Westhoff, M.C., Savenije, H.H.G., Luxemburg, W.M., Stelling, G.S., Van de Giesen, N.C., Selker, J.S., Pfister, L., Uhlenbrook, S., 2007. A distributed stream temperature model using high resolution temperature observations. Hydrol. Earth Syst. Sci. 11, 1469–1480.

Woo, M., Prowse, T.D., Ommanney, C., 1990. Permafrost hydrology. In: Northern Hydrology: Canadian Perspectives.

Woo, M.K., 2012. Permafrost hydrology, 1st ed, Permafrost Hydrology. Springer Heidelberg, Berlin. doi:10.1007/978-3-642-23462-0

Yang, D., Marsh, P., Ge, S., 2014. Heat flux calculations for Mackenzie and Yukon Rivers. Polar Sci. 8, 232–241. doi:10.1016/j.polar.2014.05.001

Zarnetske, J.P., Gooseff, M.N., Brosten, T.R., Bradford, J.H., McNamara, J.P., Bowden, W.B., 2007. Transient storage as a function of geomorphology, discharge, and permafrost active layer conditions in Arctic tundra streams. Water Resour. Res. 43, 1–13. doi:10.1029/2005WR004816

Zhang, T., Barry, R.., Knowles, K., Ling, F., Armstrong, R.L., 2003. Distribution of seasonally and perennially frozen ground in the Northern Hemisphere, in: ICOP 2003 Permafrost: Proceedings of the 8th International Conference on Permafrost. A.A. Balkma, Netherlands, pp. 1289–1294.

Figures

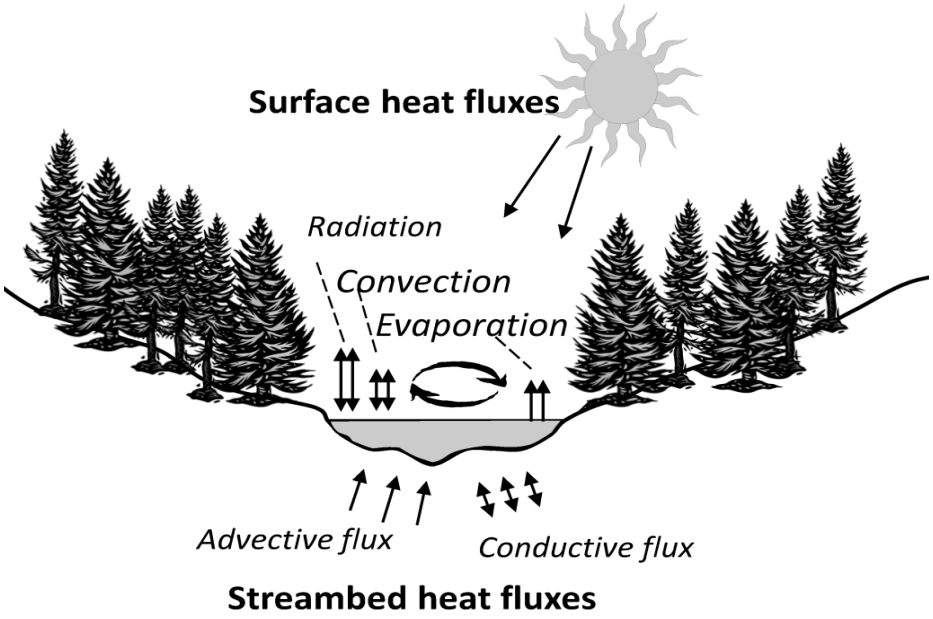

Figure 1.1 Heat fluxes across the streambed and surface contributing to the energy balance of a gaining stream (Kurylyk et al., 2015).

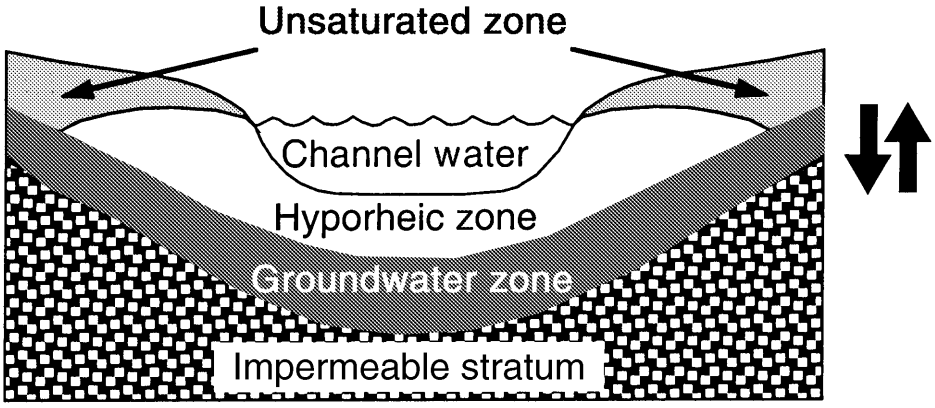

Figure 1.2 Conceptual diagram showing the idealized location of the hyporheic zone beneath a stream channel. Arrows indicate bidirectional fluxes of water between the stream, and hyporheic and groundwater zones. Adapted from Malard et al. (2002).

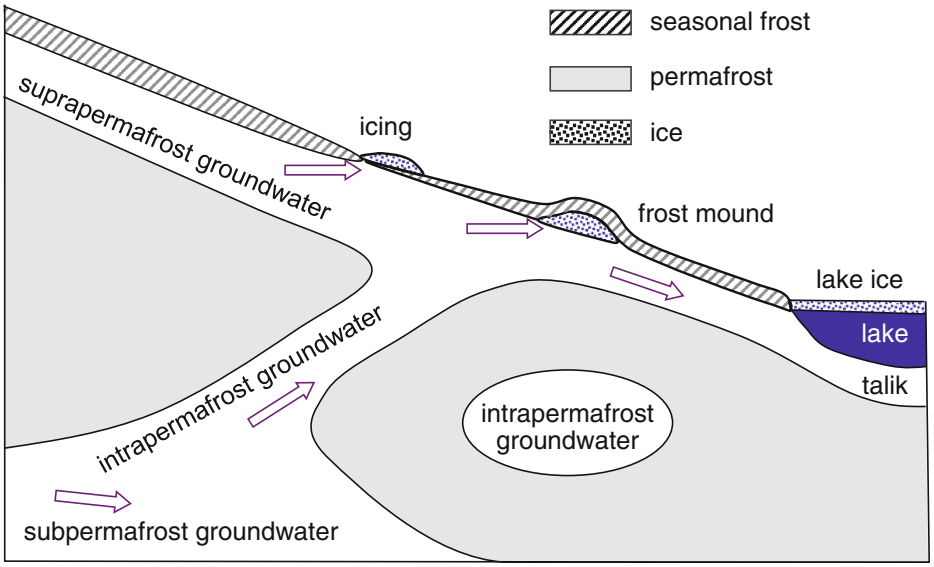

Figure 1.3 Conceptual diagram illustrating the various types of groundwater found in permafrost regions (Woo, 2012).

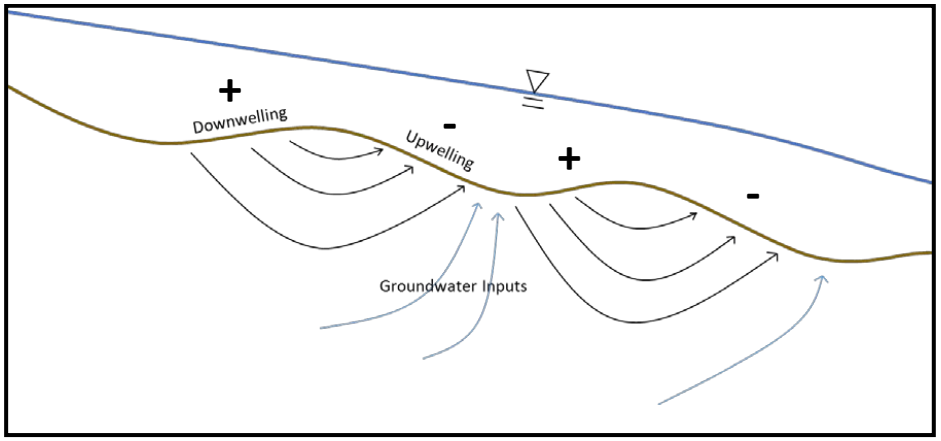

Figure 1.4 Conceptual diagram of hyporheic exchange in pool-riffle complexes under the influence of hydraulic head differences. + indicates high head, - indicates low head. Adapted from Kraseski (2015).

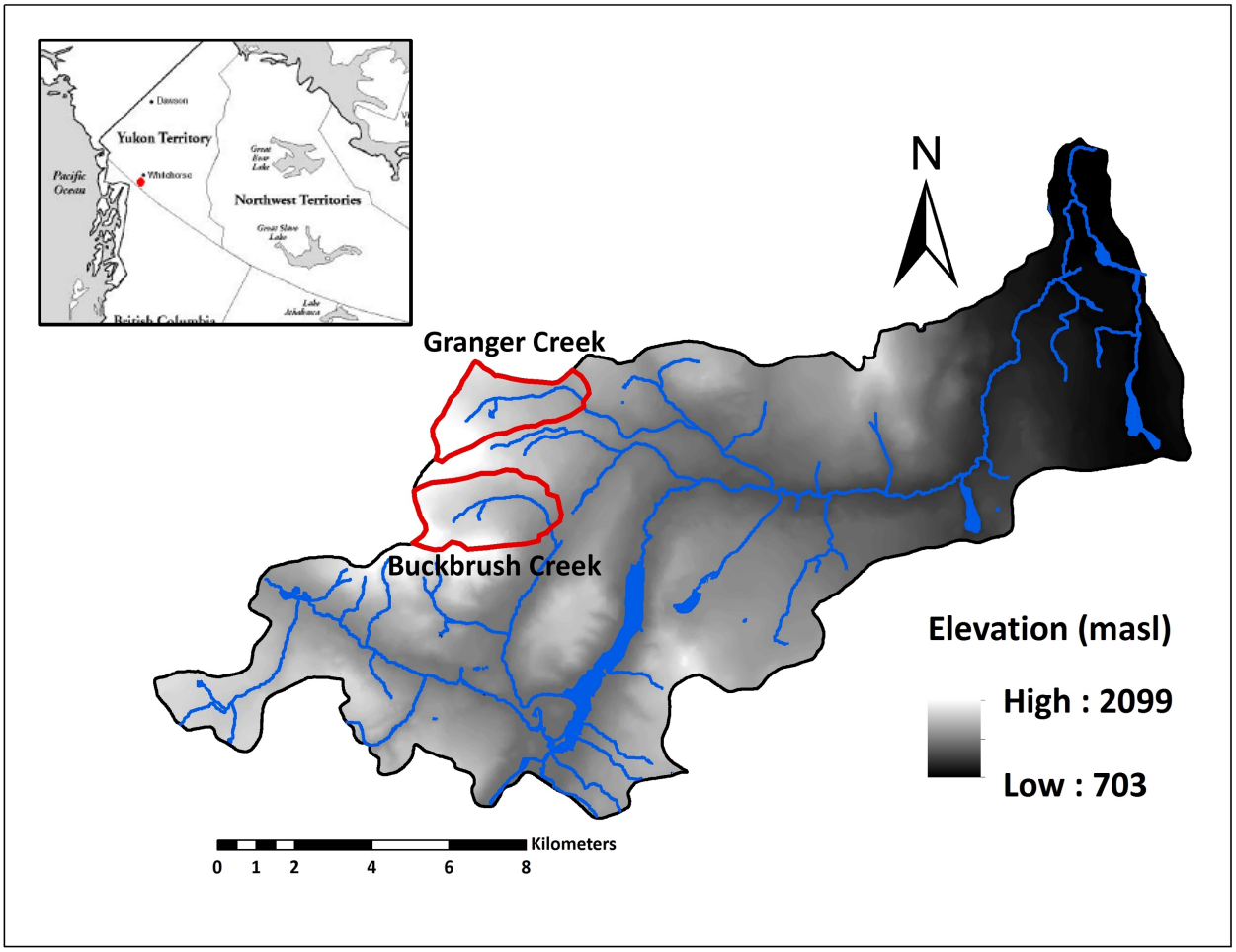

Figure 2.1 Location and topography of the study catchments, Granger Creek (GC) and Buckbrush Creek (BB) within the Wolf Creek Research Basin (WCRB). Respective drainage areas are delineated by the red lines. Inset map shows the location of WCRB in the Yukon Territory.

Figure 2.2 Lower (a) and upper reaches (b) of BB, and a temperature sensor located in a large pool (c).

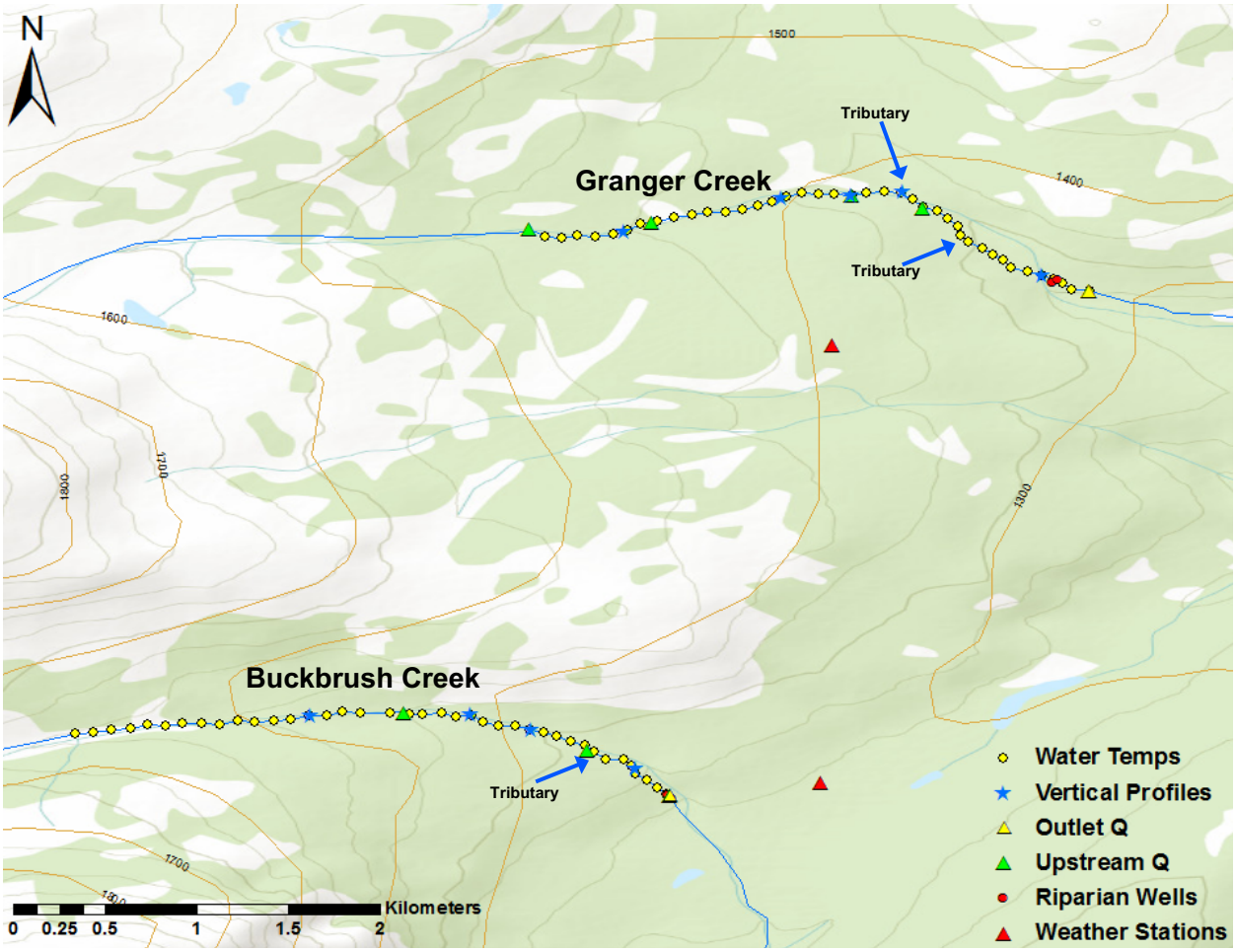

Figure 2.3 Sample locations in GC and BB.

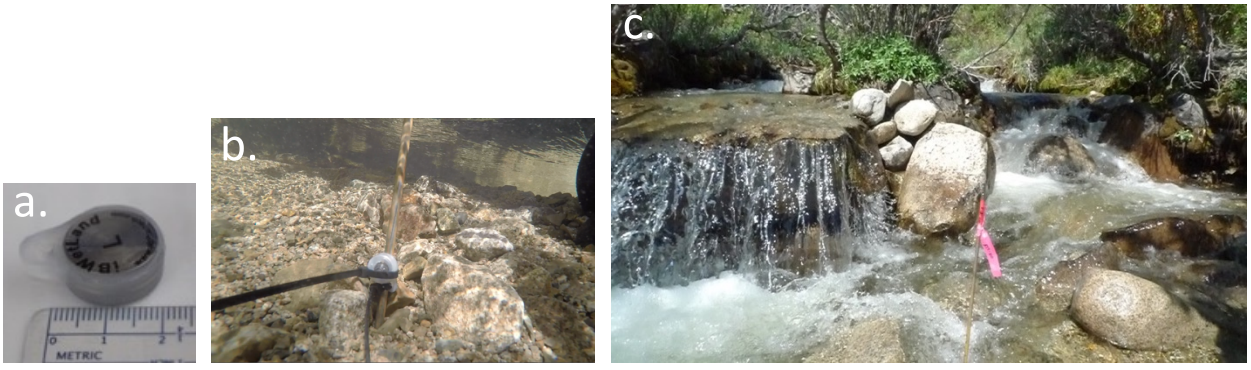

Figure 2.4 iButtons (a) mounted at the sediment-water interface (b), centre-channel (c).

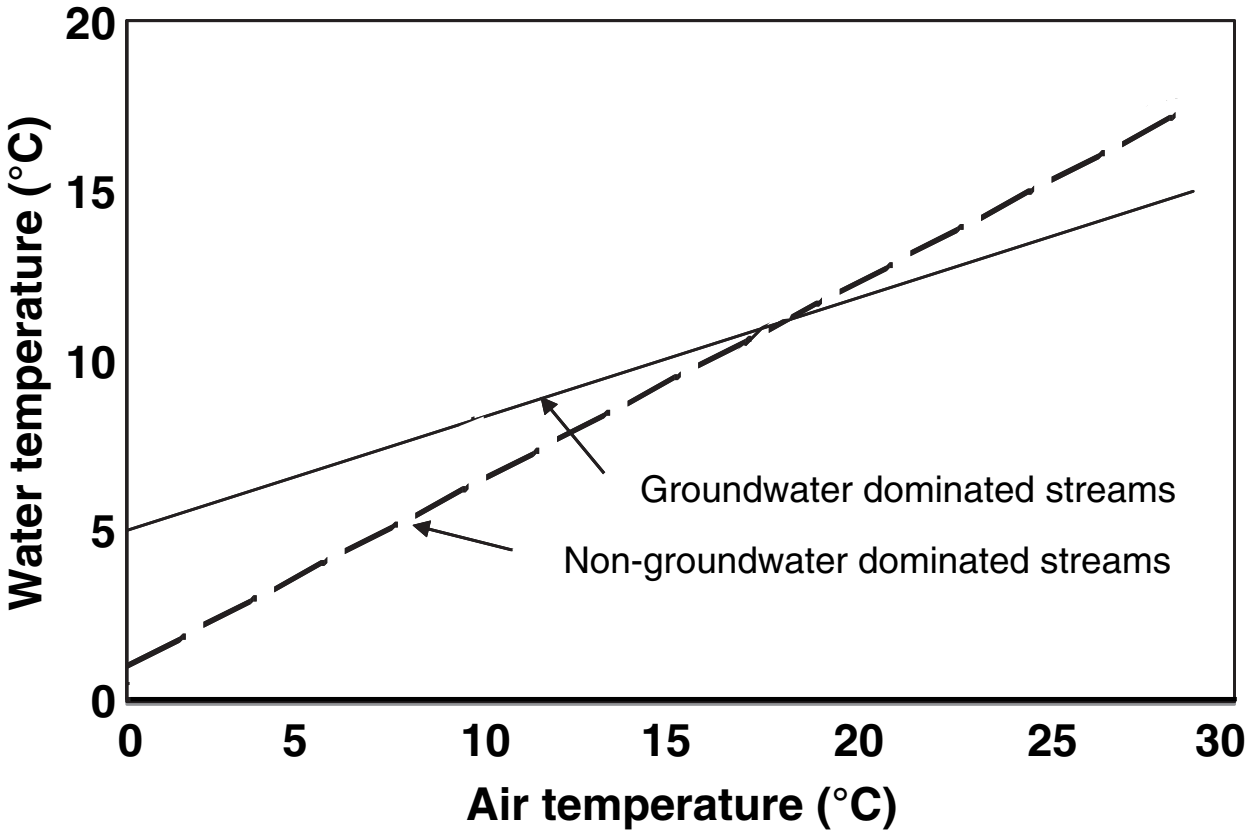

Figure 2.5 Example of simple air temperature-water temperature linear regression highlighting the differences between groundwater and non-groundwater dominated streams. Adapted from Caissie (2006).

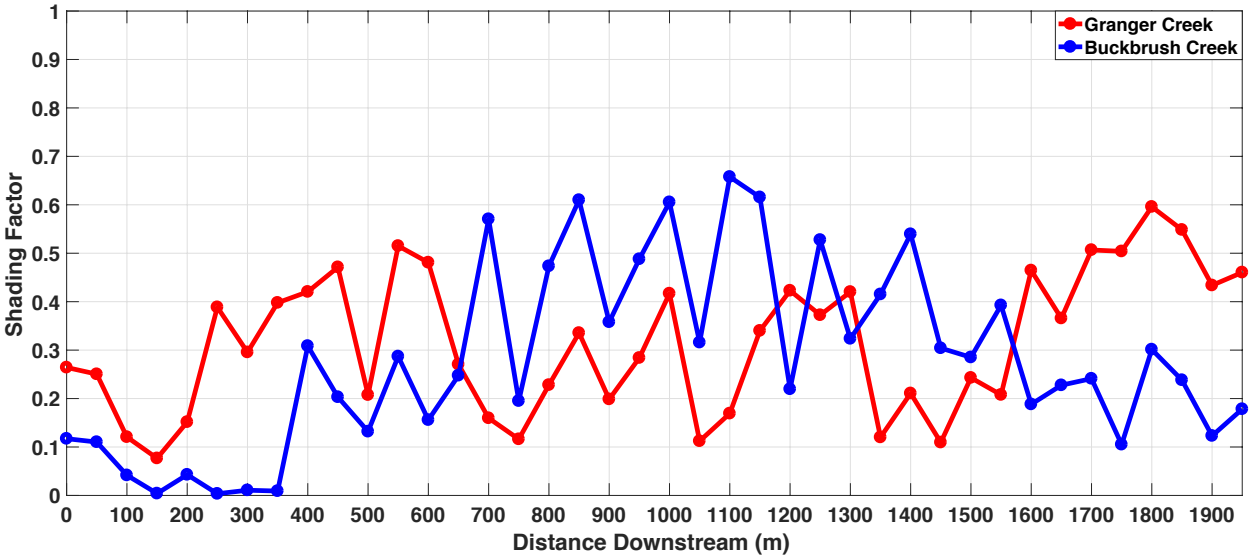

Figure 2.6 Longitudinal plots of shading factor (0 to 1, or no canopy to full canopy, respectively) with distance downstream in GC and BB.

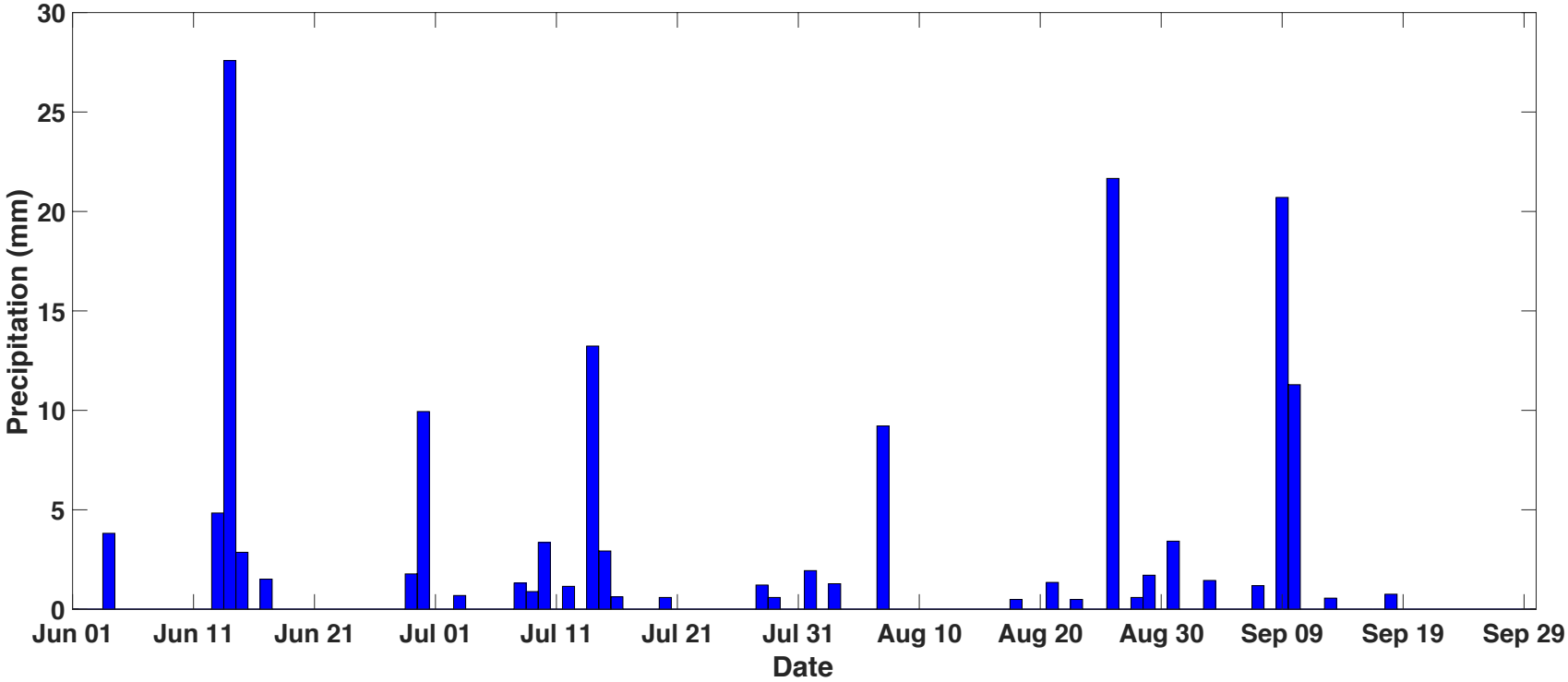

Figure 3.1 Precipitation in the WCRB over the study period (June to September 2016).

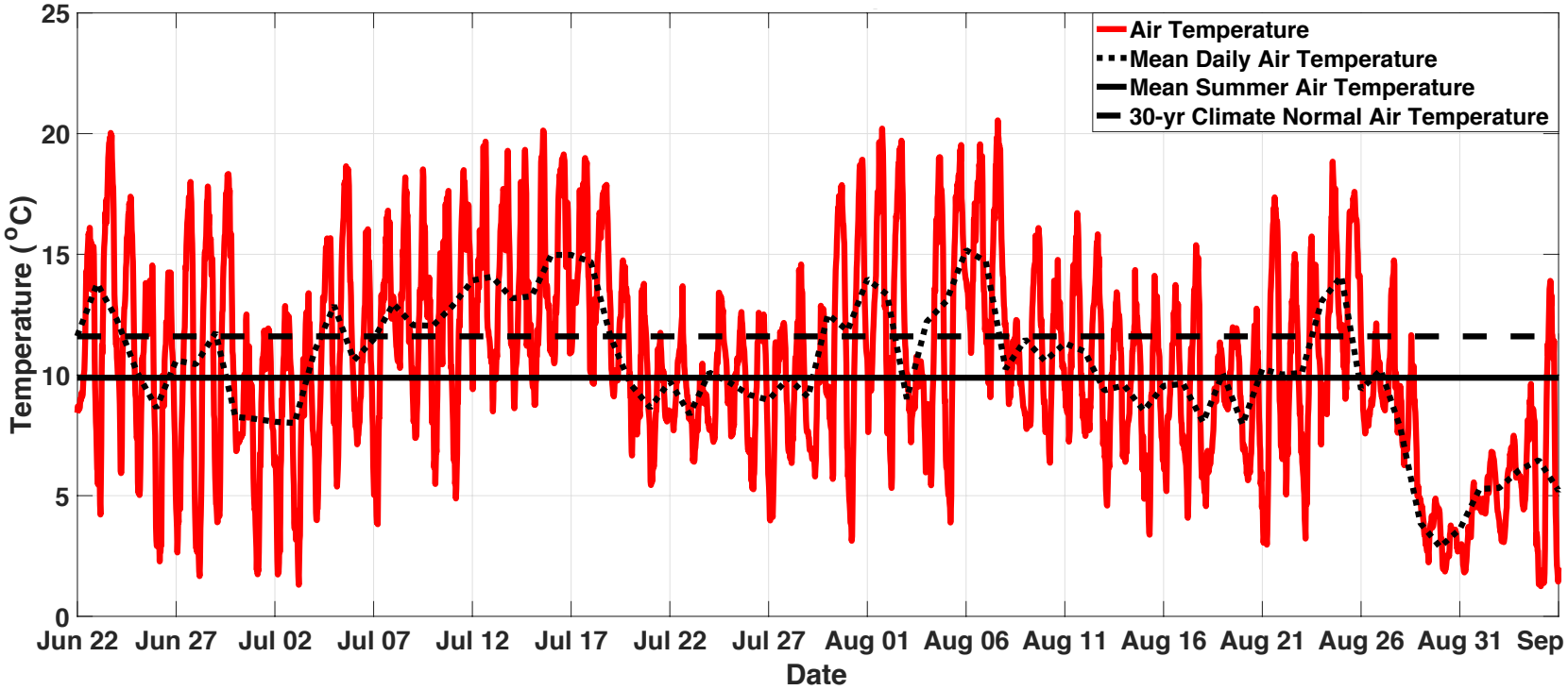

Figure 3.2 Continuous, mean daily, mean summer, and 30-yr mean air temperature in the WCRB over the study period.

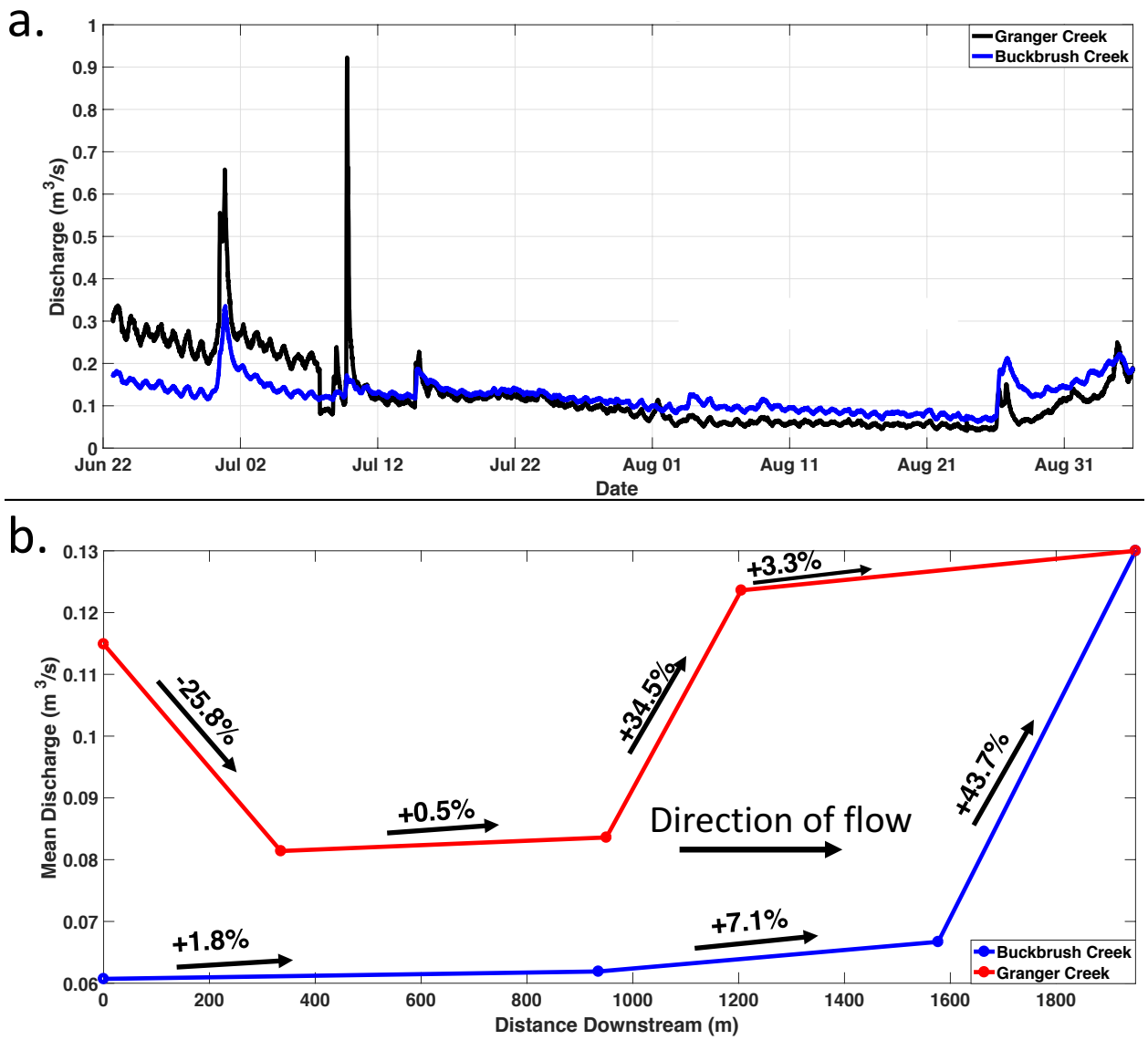

Figure 3.3 Outlet hydrographs for GC and BB (a) and plots of mean study period discharge with distance downstream indicating percent change in discharge between stations (b).

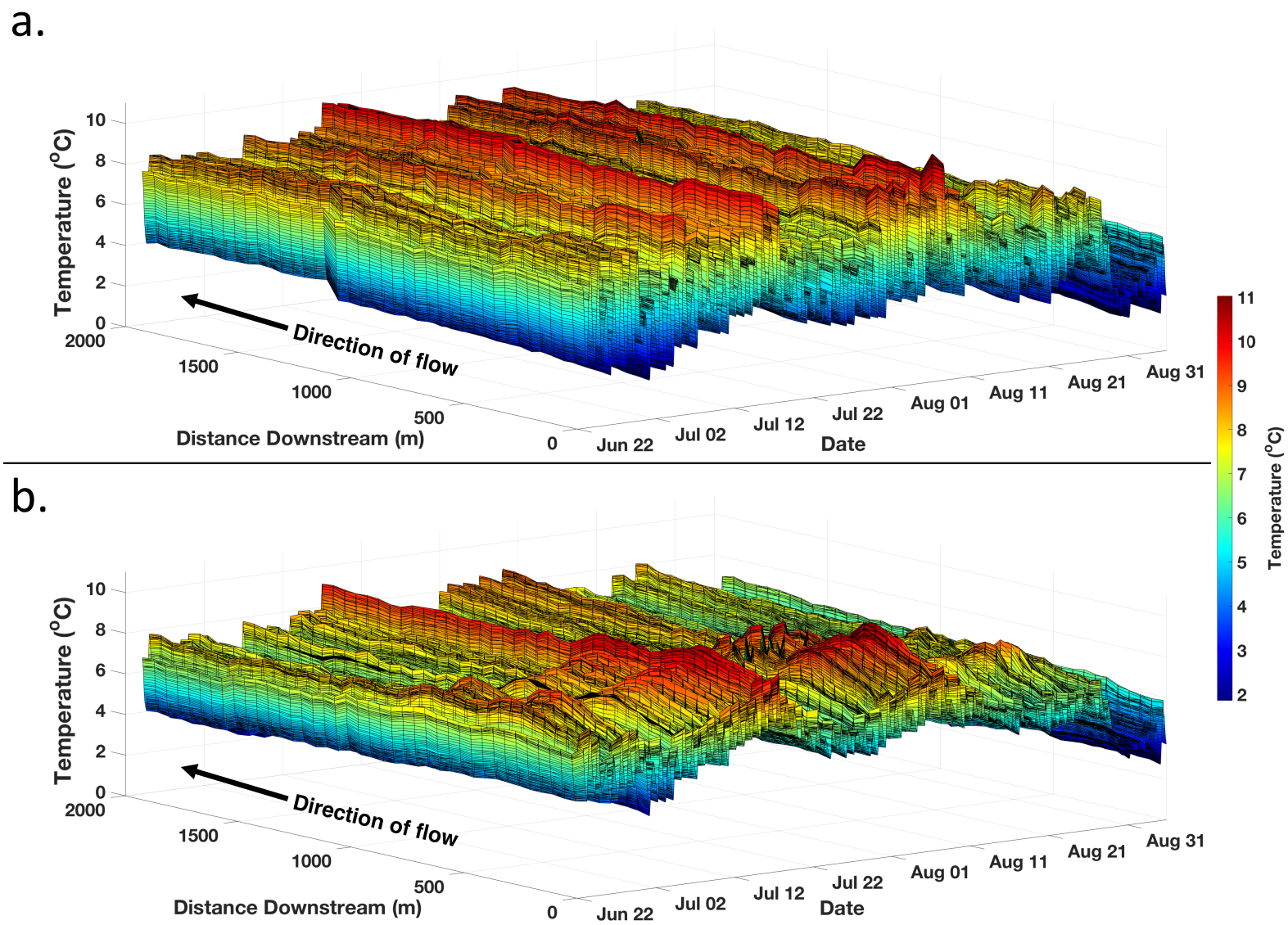

Figure 3.4 Temperature (y) with time (x) and distance (z) in GC (a) and BB (b) over the study period (June 22 to September 05, 2016).

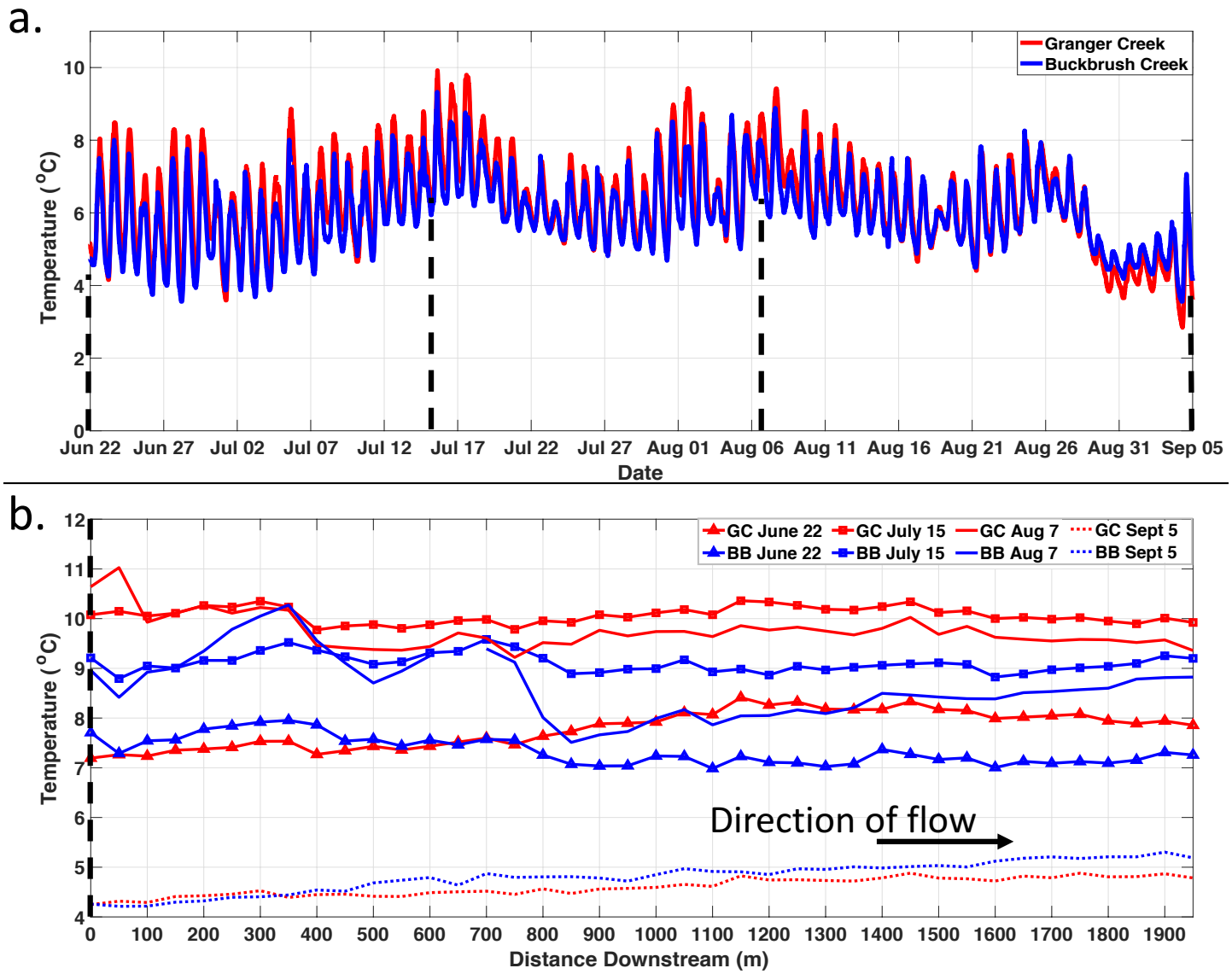

Figure 3.5 Summer stream temperatures (a) and longitudinal temperature profiles at 15:00 on four days over the study period (b) at the outlets of GC and BB. The black dotted lines in a) indicate the times of measurement in b), the black dotted line in b) indicates the sensor location that temperature was recorded at in a).

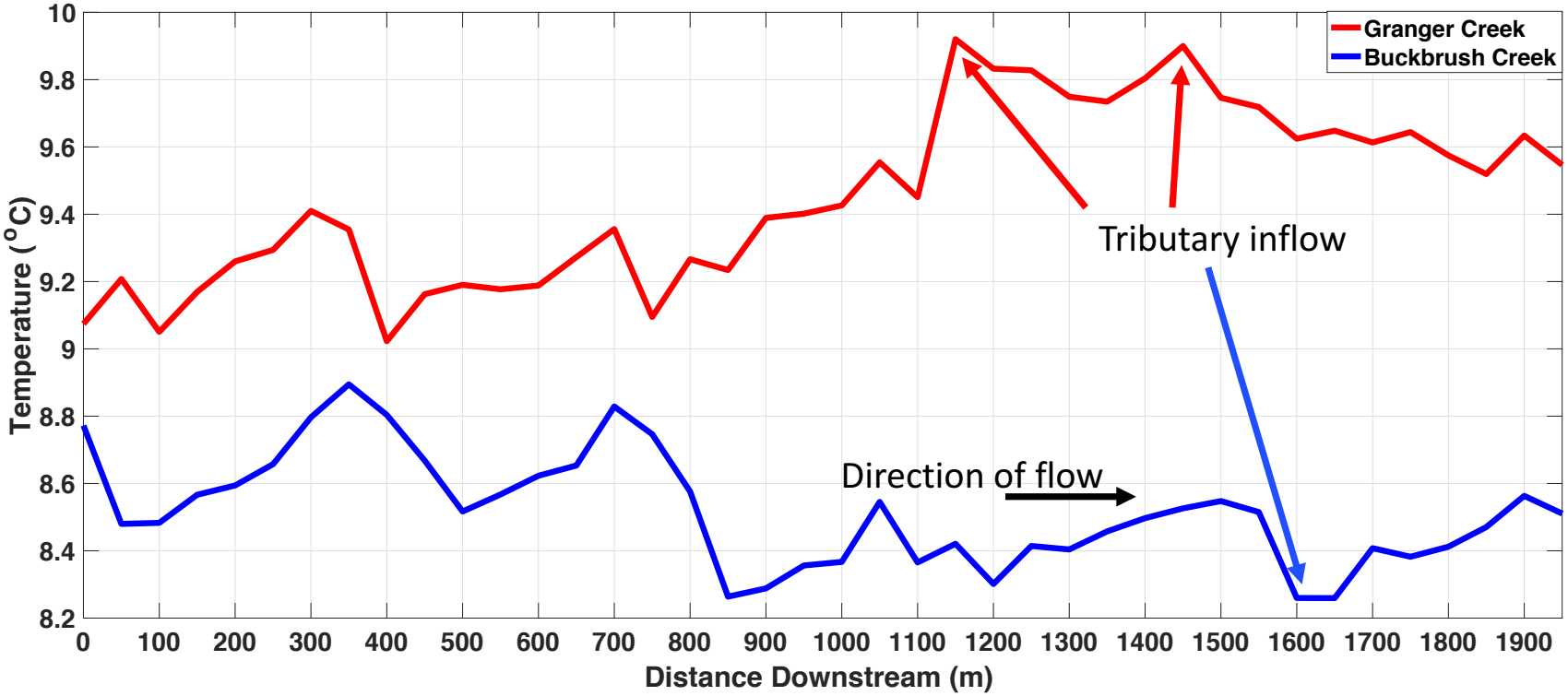

Figure 3.6 Longitudinal temperature profiles at 16:00 on the warmest day of the summer (July 15) in GC and BB highlight the difference in downstream temperature development in each stream. The red (blue) arrows indicate the warming (cooling) effect of tributary inflow to GC (BB).

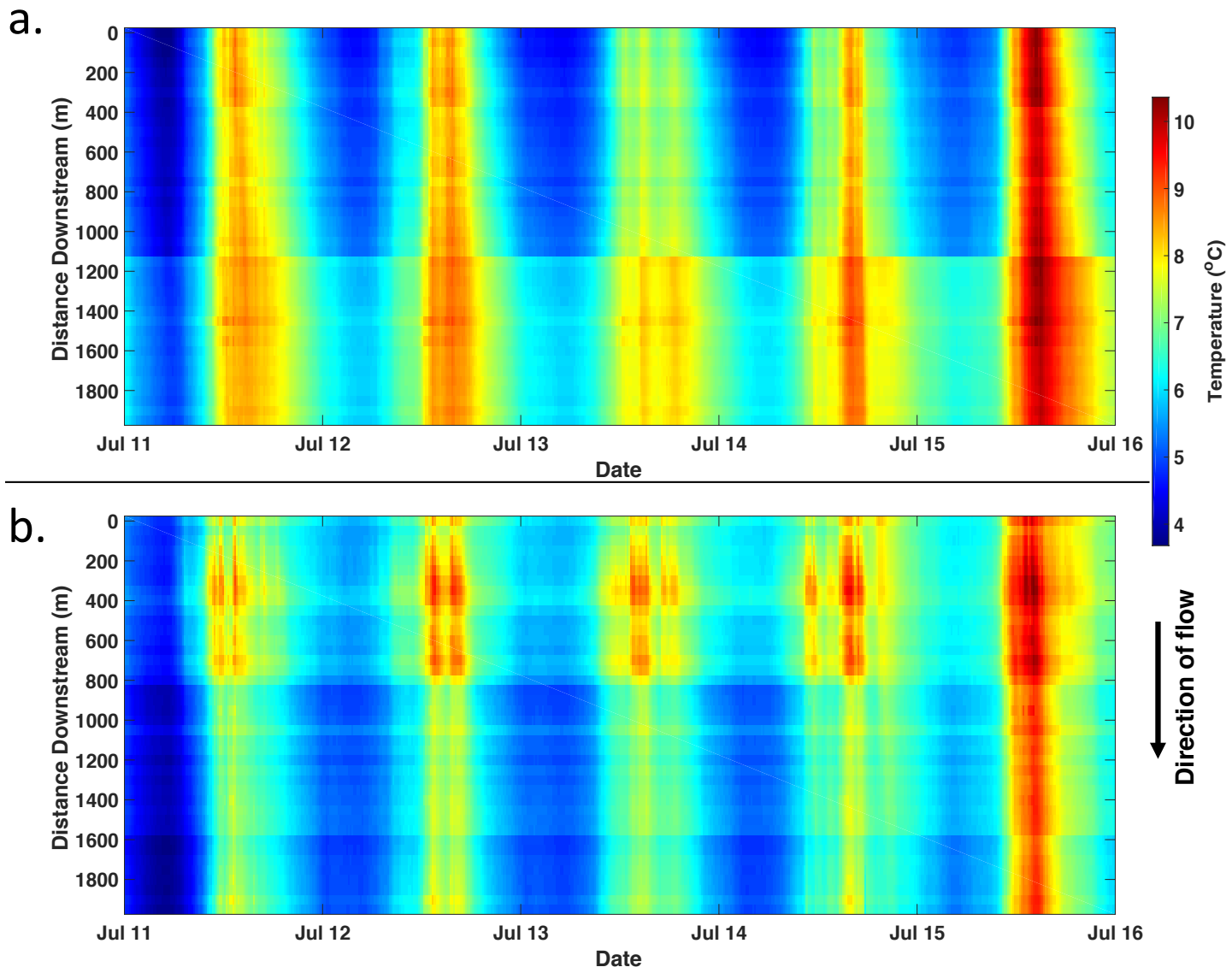

Figure 3.7 Temperature with time (x) and distance (y) in GC (a) and BB (b) during part of the warmest period of the study season (July 11 – 16).

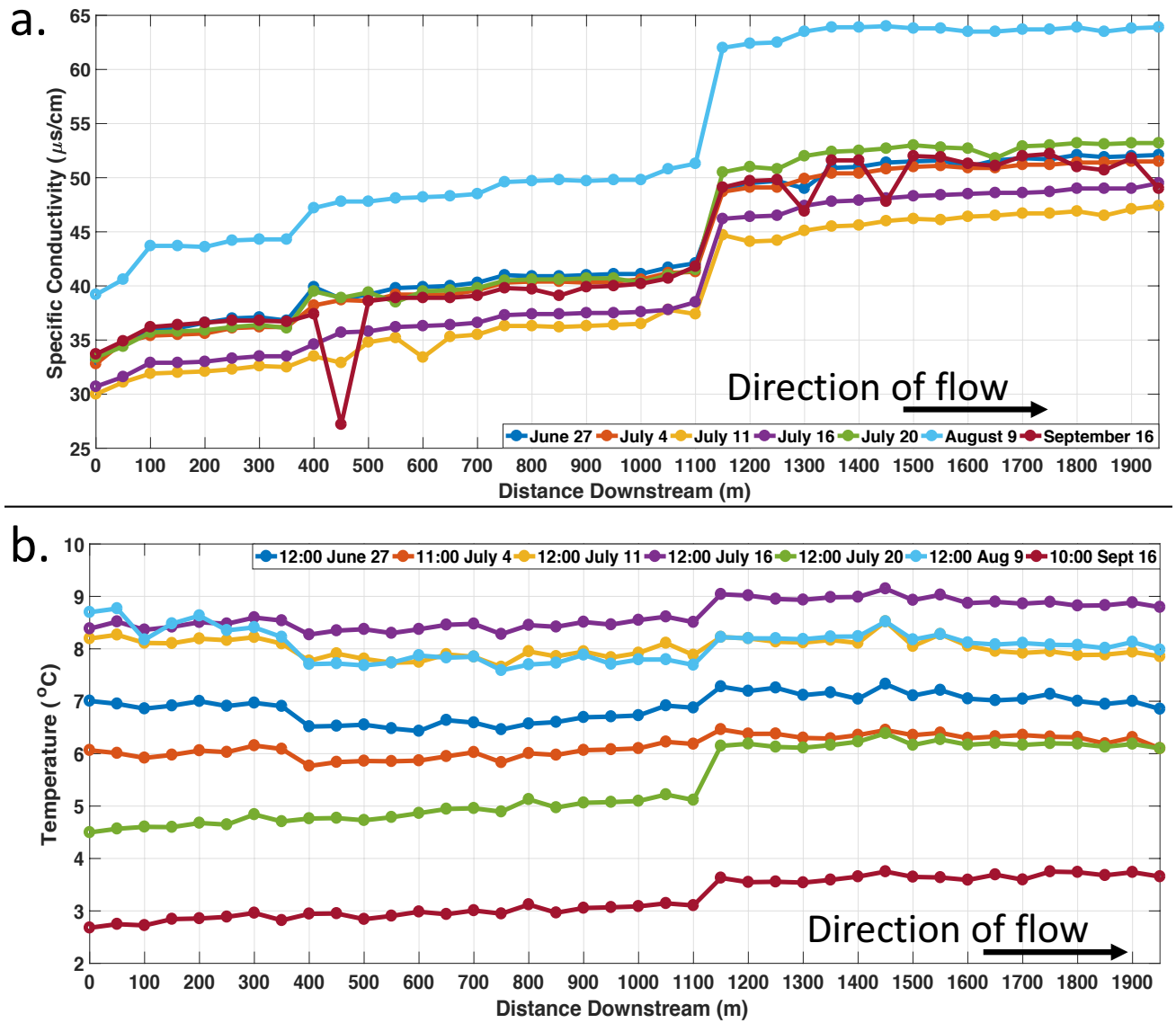

Figure 3.8 Comparison of longitudinal trends in specific conductivity (a) and temperature (b) in GC.

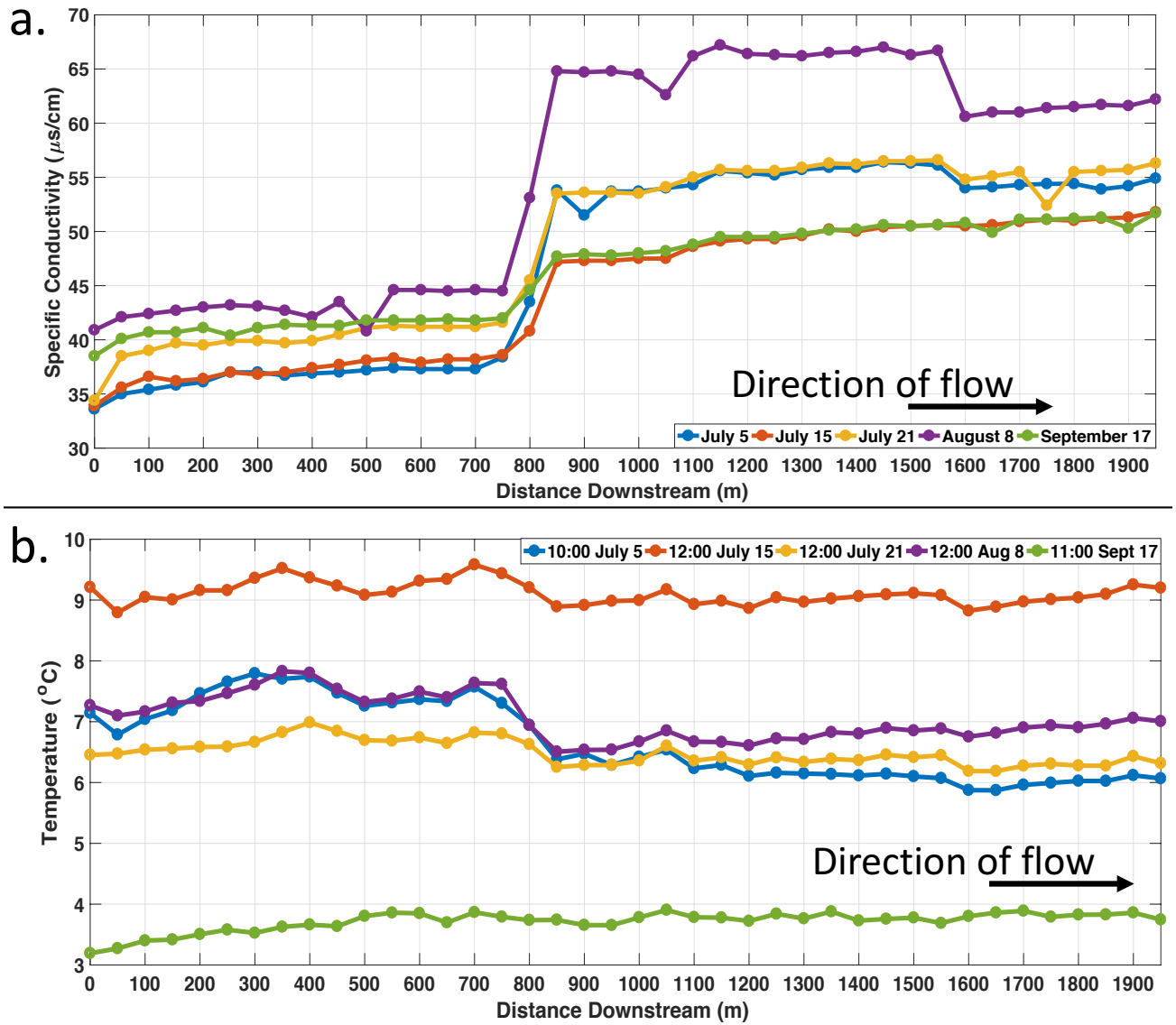

Figure 3.9 Comparison of longitudinal trends in specific conductivity (a) and temperature (b) in BB.

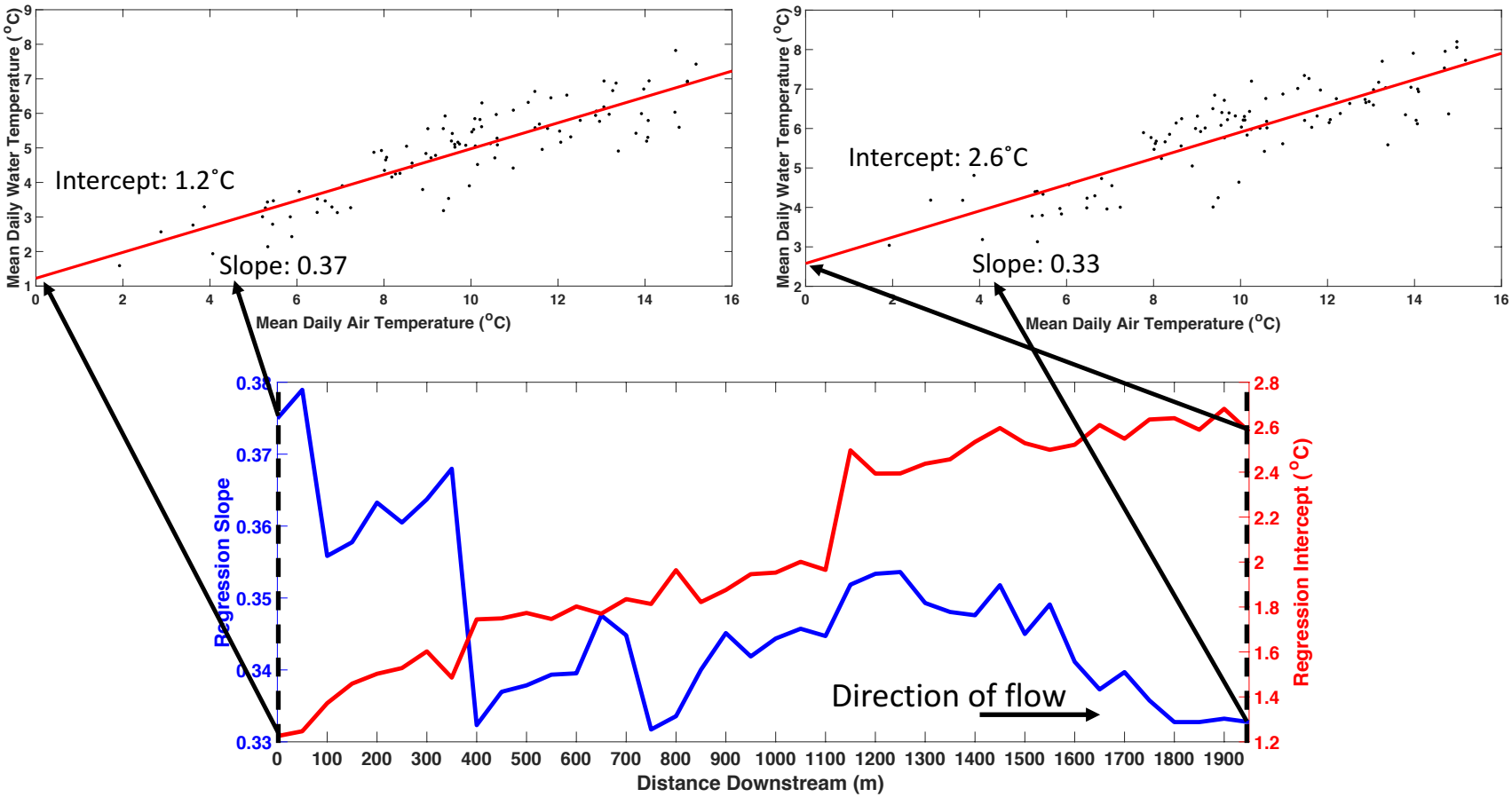

Figure 3.10 Longitudinal plots of regression slope and intercept at each sampling location in GC. The nested plots above display the regressions performed at the sensor location indicated by the black dotted line.

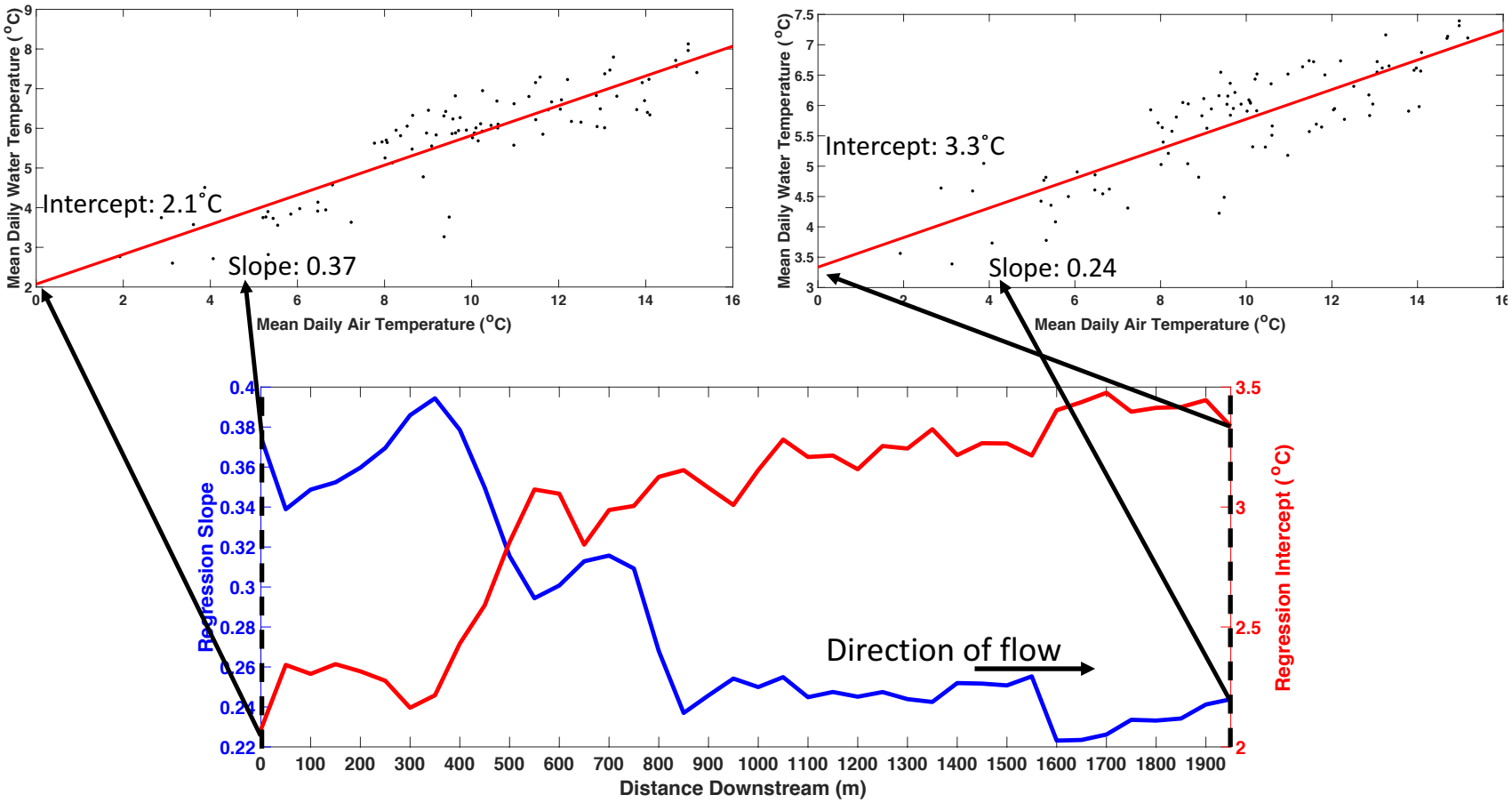

Figure 3.11 Longitudinal plots of regression slope and intercept at each sampling location in BB. The nested plots above display the regressions performed at the sensor location indicated by the black dotted line.

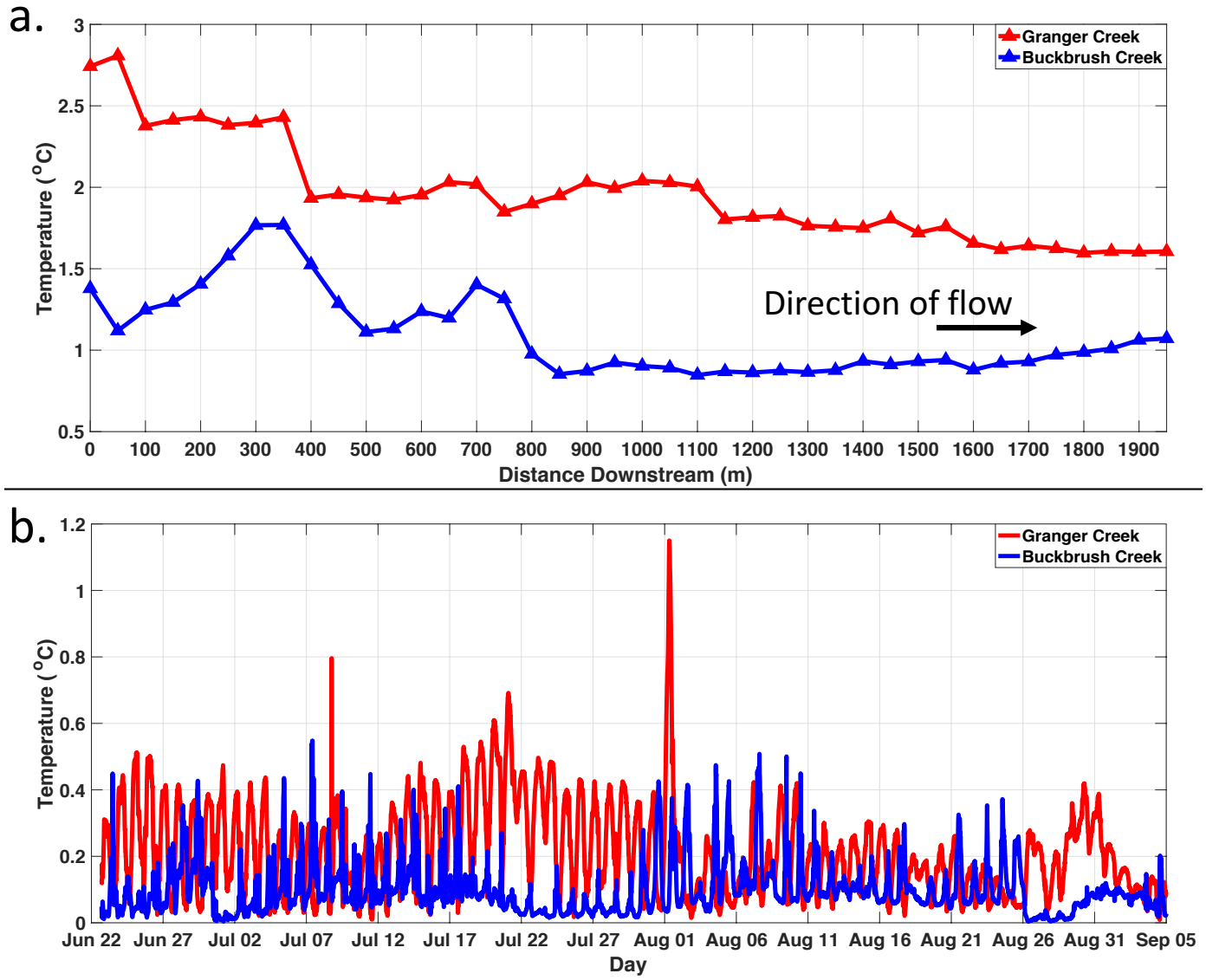

Figure 3.12 Spatial temperature variance with distance downstream in GC and BB (a) and study reach temporal temperature variance in GC and BB over the study period (June 22 to Sept 05, 2016) (b).

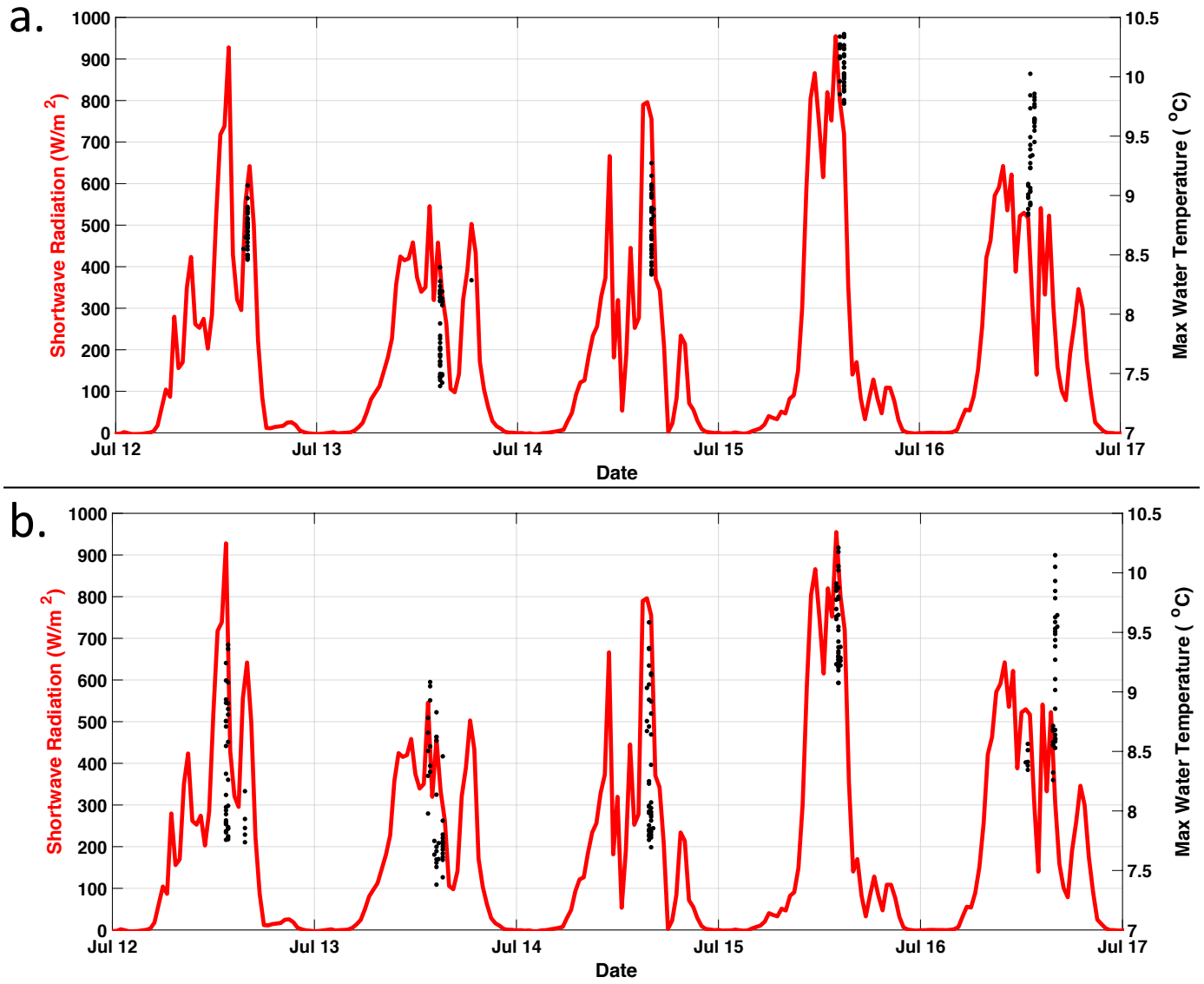

Figure 3.13 Incoming shortwave radiation and maximum daily water temperature at each sensor location in GC (a) and BB (b) during the warmest period of the season shows synchroneity between timing of peak radiation and maximum daily water temperature.

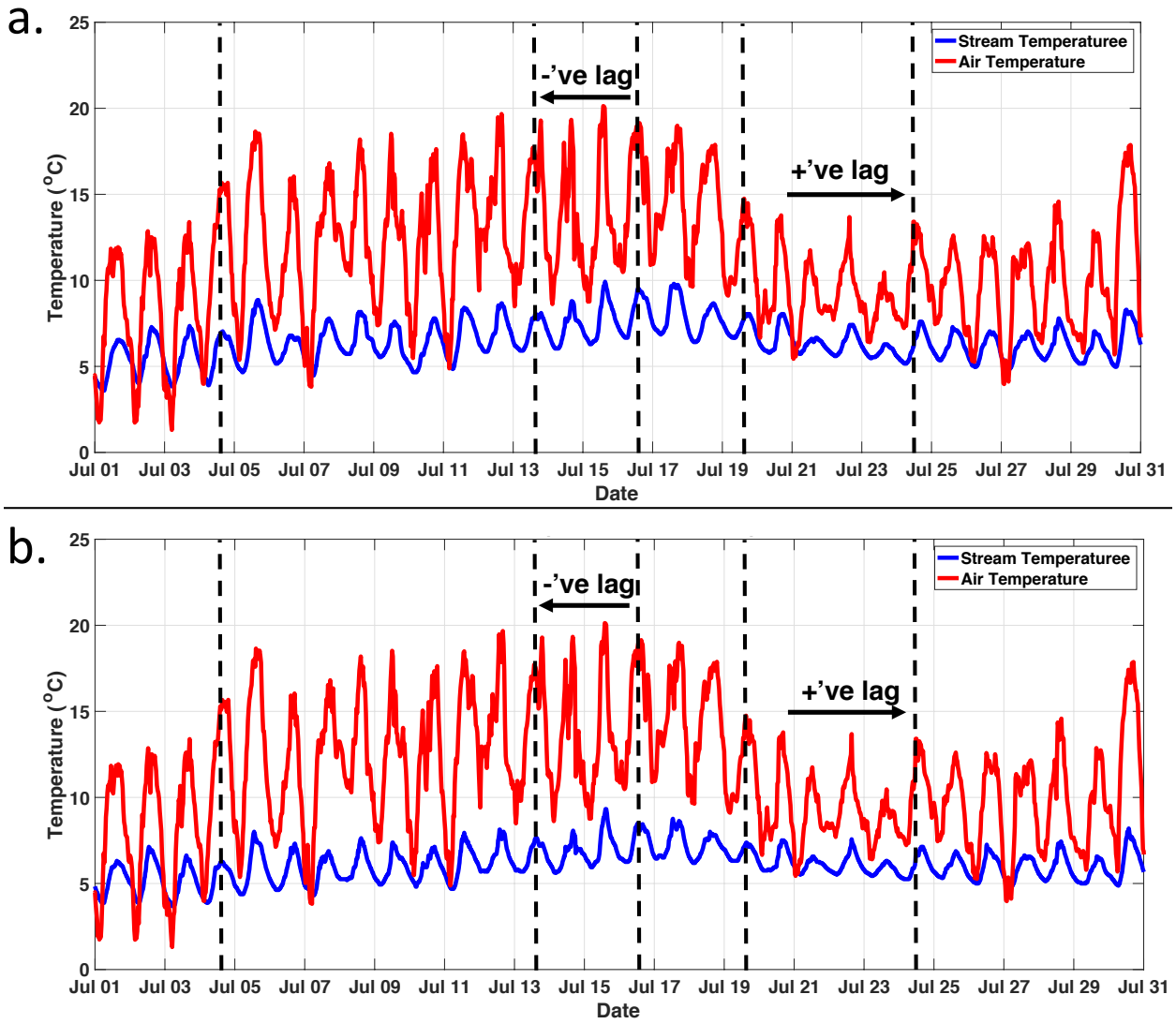

Figure 3.14 Comparison of air temperature and water temperature at the 'outlet' locations (1950 m downstream) in GC (a) and BB (b) in July 2016 shows the occurrence of positive lags (air temperature peaks first) and negative lags (water temperature peaks first). Several occurrences of either positive or negative lags are indicated with vertical dotted lines. This occurs along the length of each stream and throughout the season, with more negative lags in July and more positive lags in August (Figure 3.15).

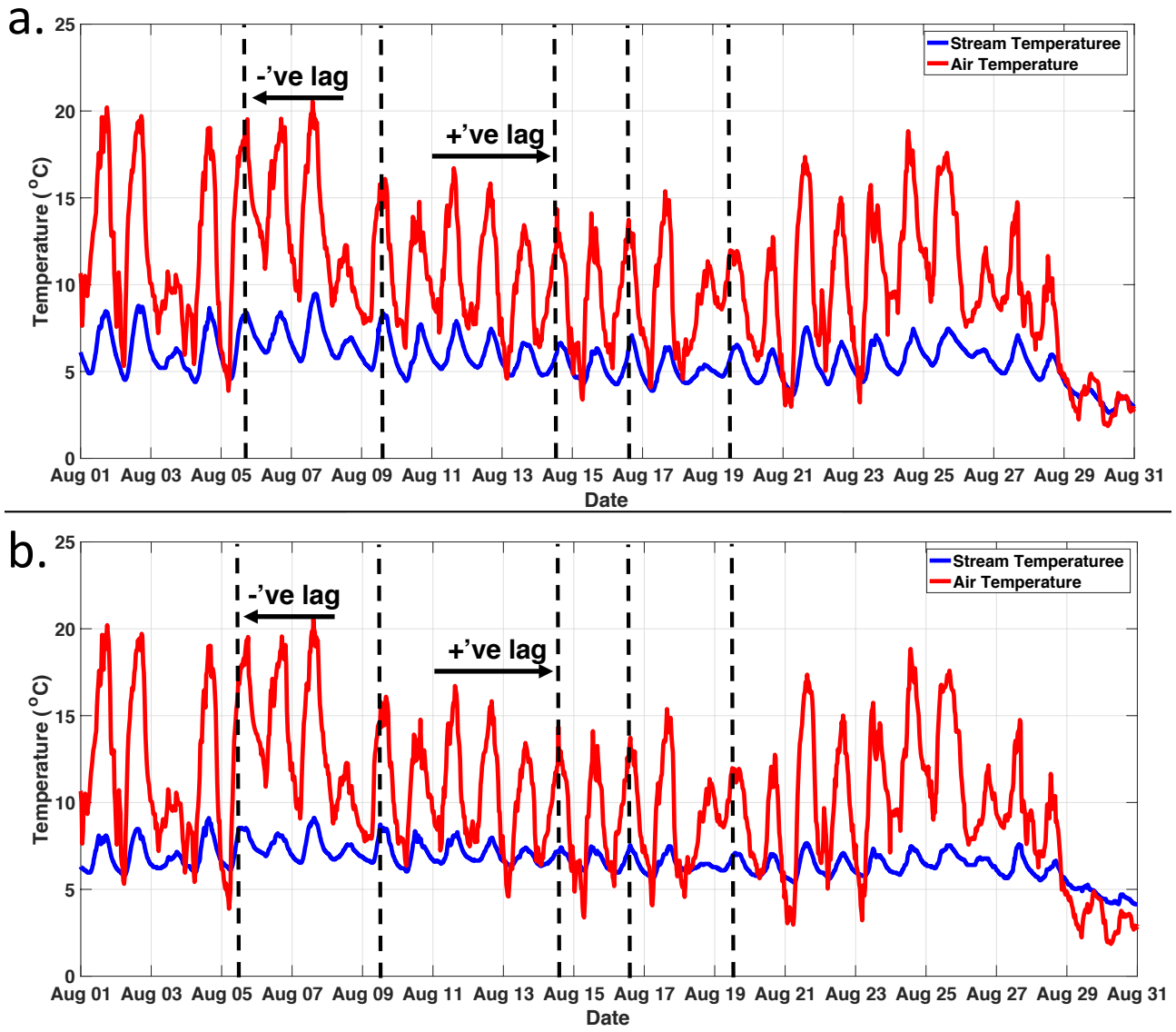

Figure 3.15 Comparison of air temperature and water temperature at 450 m downstream in GC (a) and BB (b) in August 2016 shows the occurrence of positive lags (air temperature peaks first) and negative lags (water temperature peaks first). Several occurrences of either positive or negative lags are indicated with vertical dotted lines.

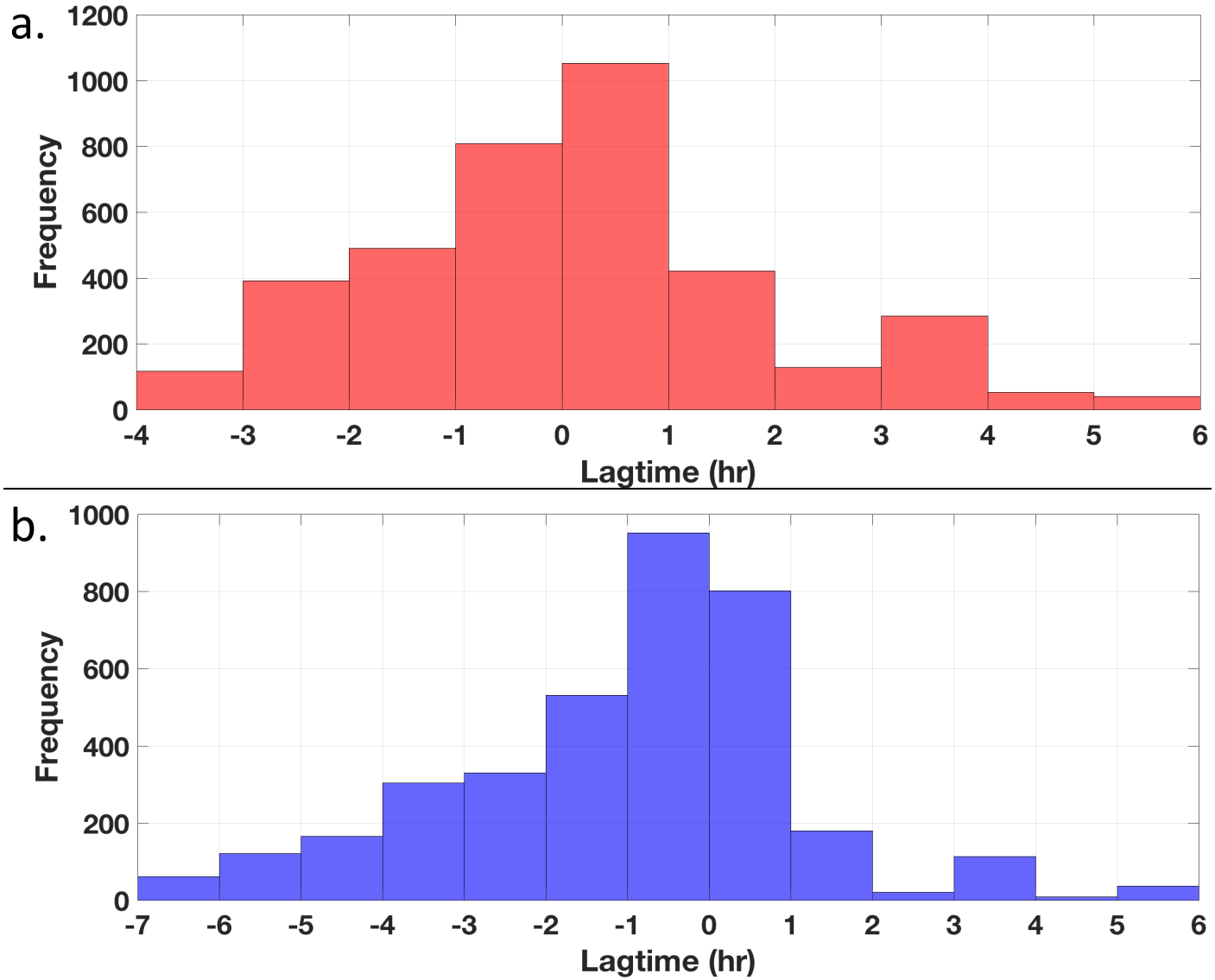

Figure 3.16 Frequency of lags between daily maximum air and water temperature at the study reach outlets in GC (a) and BB (b).

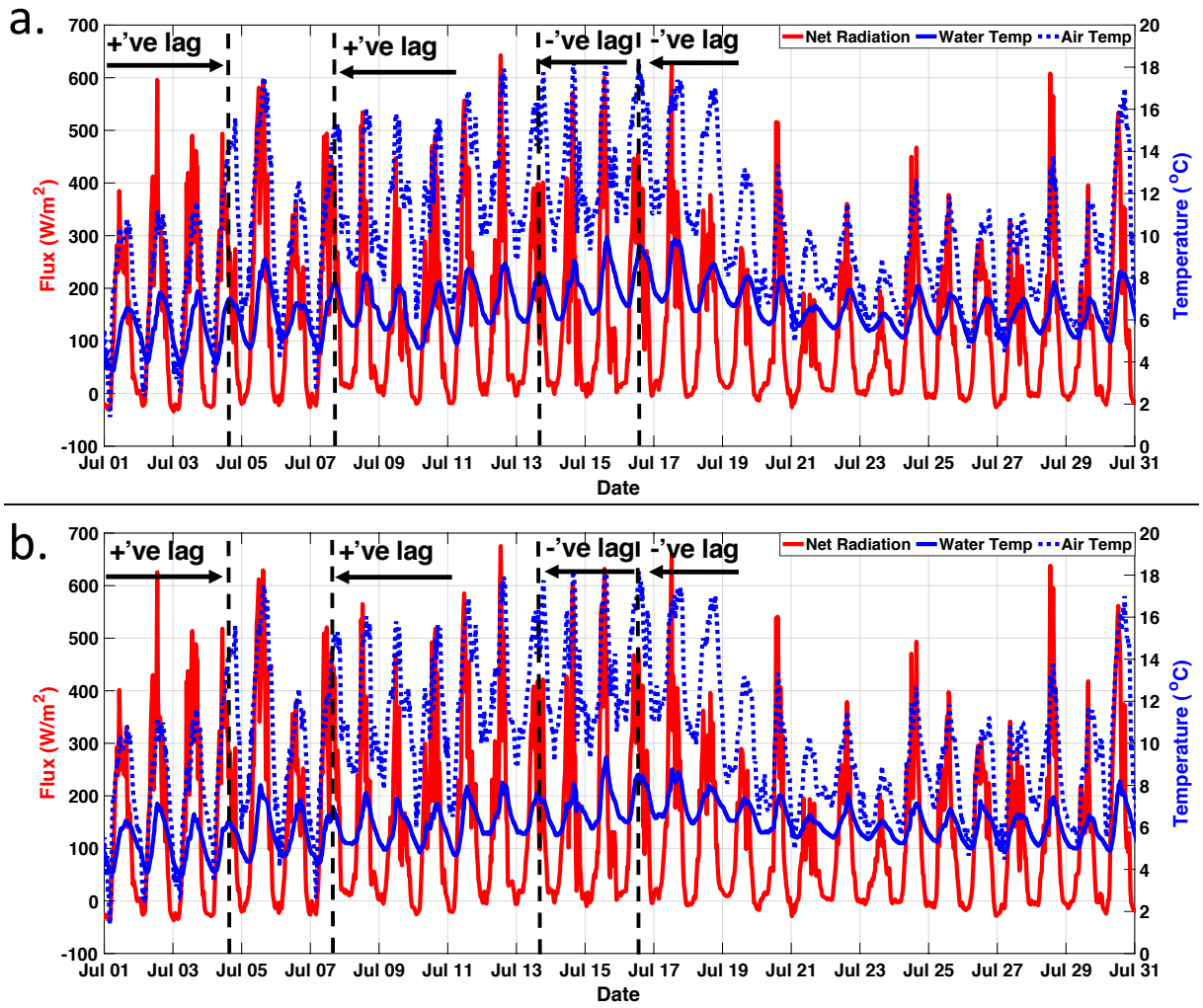

Figure 3.17 Comparison of net radiation, air temperature, and water temperature at the 'outlet' locations (1950 m downstream) in GC (a) and BB (b) in July 2016 shows that negative lags (water temperature peaks first) between net radiation and water temperature do occur, but less so than negative air-water temperature lags. Several occurrences of either positive or negative lags are indicated with vertical dotted lines. Air temperature has been included to illustrate that although a negative air-water temperature lag occurs, a positive net radiation-water temperature lag can also occur (July 4 and 7 in both a and b).

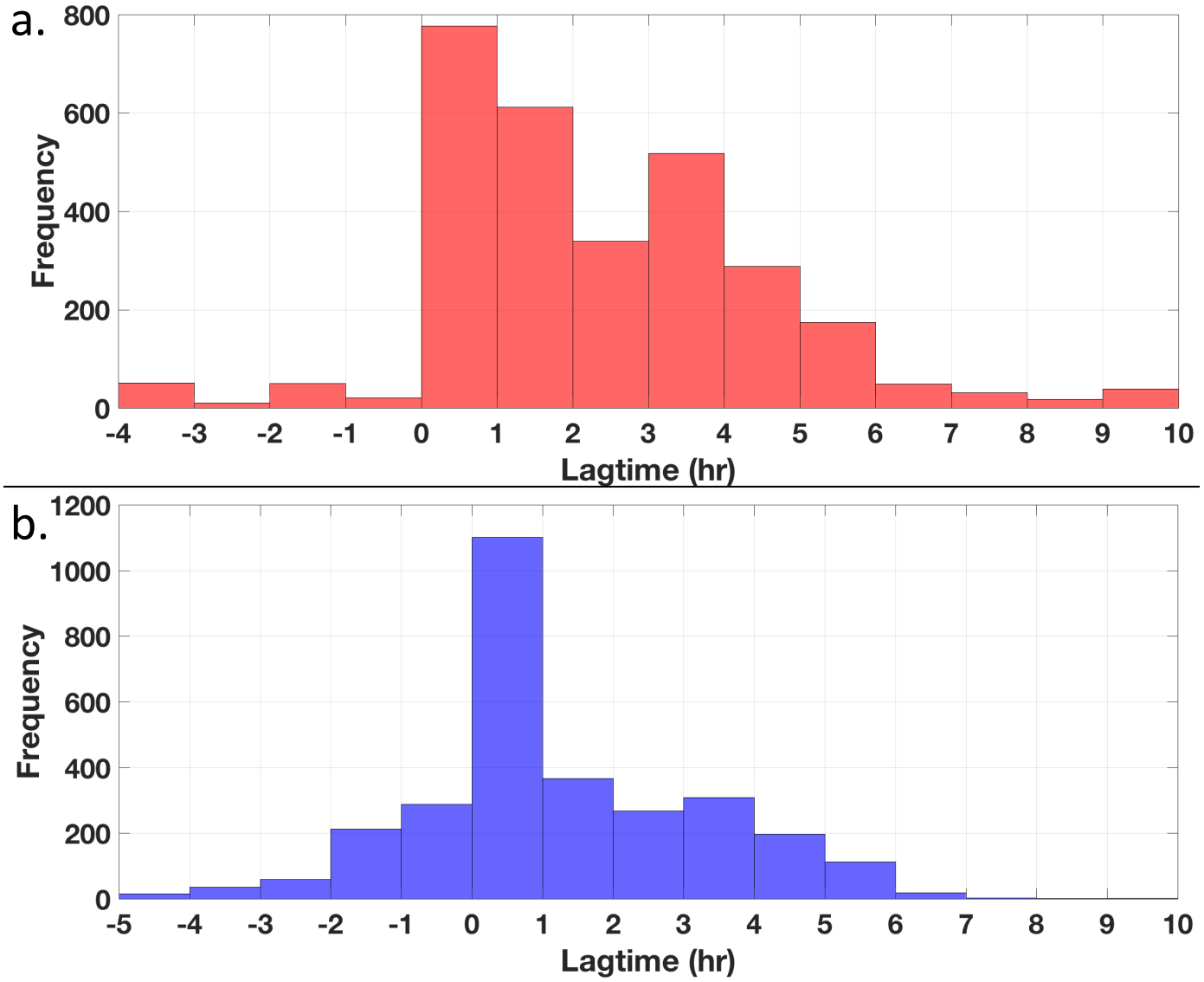

Figure 3.18 Frequency of lags between daily maximum net radiation and water temperature at the study reach 'outlets' (1950 m downstream) in GC (a) and BB (b).

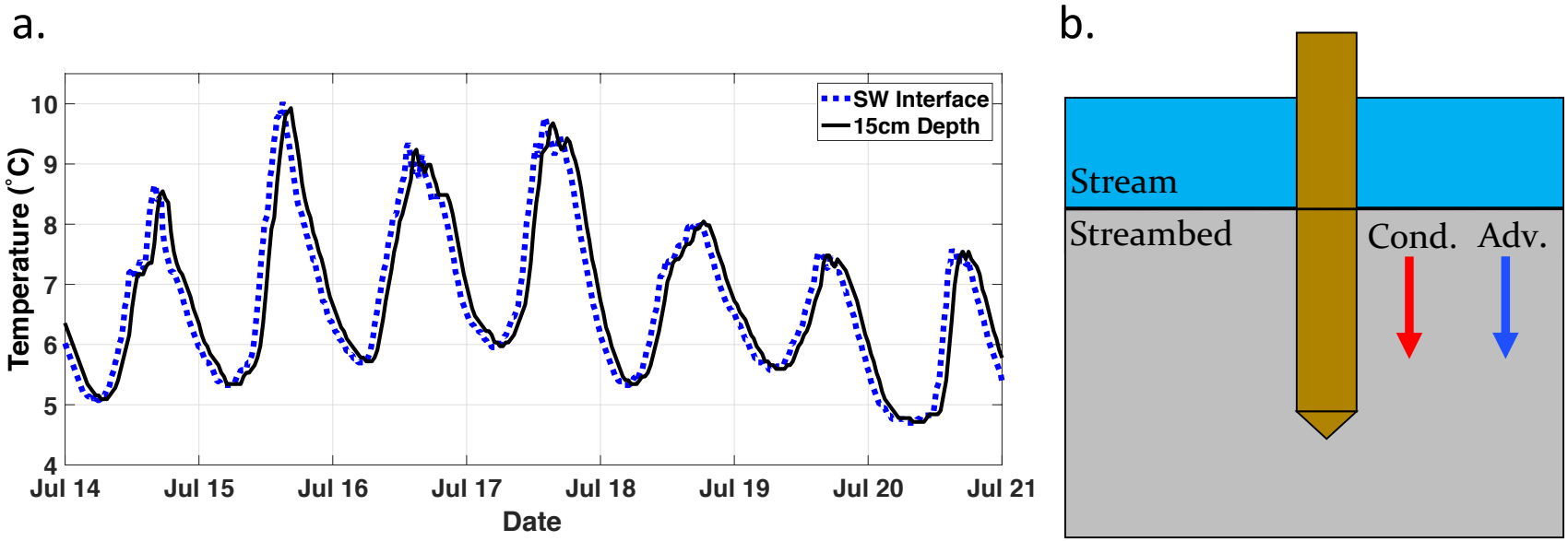

Figure 3.19 Vertical streambed temperature (a) at 950 m downstream in GC shows very little shift or damping of the temperature signal with depth. This is seen at every vertical temperature time-series location in both Granger Creek and Buckbrush Creek throughout the study period. An illustration shows the common direction of both conduction and advection under the influence of downwelling (b), this occurrence results in the negligible lag and damping of the temperature signal with depth seen in (a).

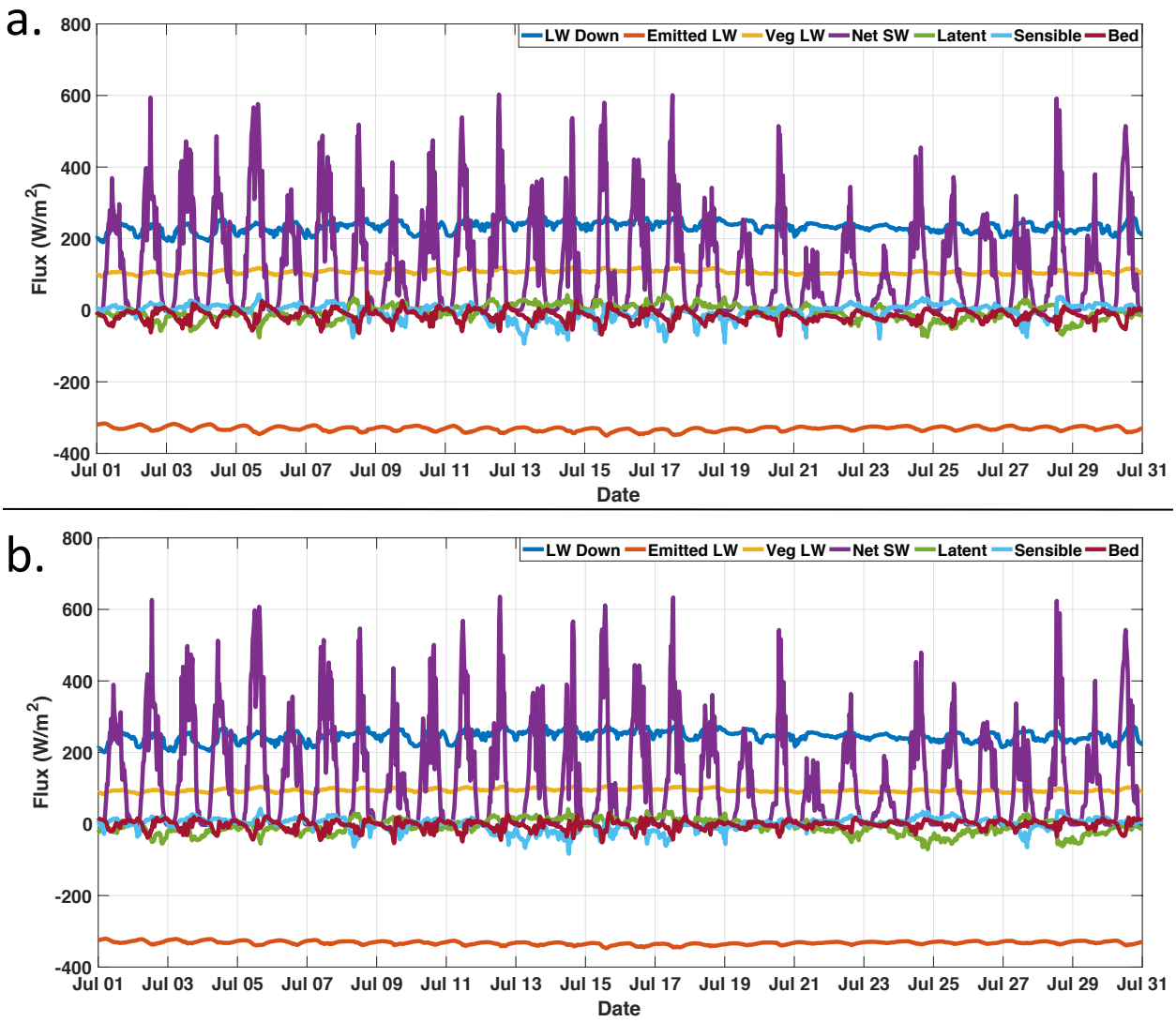

Figure 3.20 Distributed energy fluxes averaged over the study reaches (1950 m) for July 2016 in GC (a) and BB (b). LW Down is incoming longwave radiation, Emitted LW is longwave radiation emitted by the stream surface, Veg LW is longwave radiation emitted by vegetation, Net SW is net shortwave radiation, Latent is the latent heat flux, Sensible is the sensible heat flux, and Bed is the bed conductive heat flux.

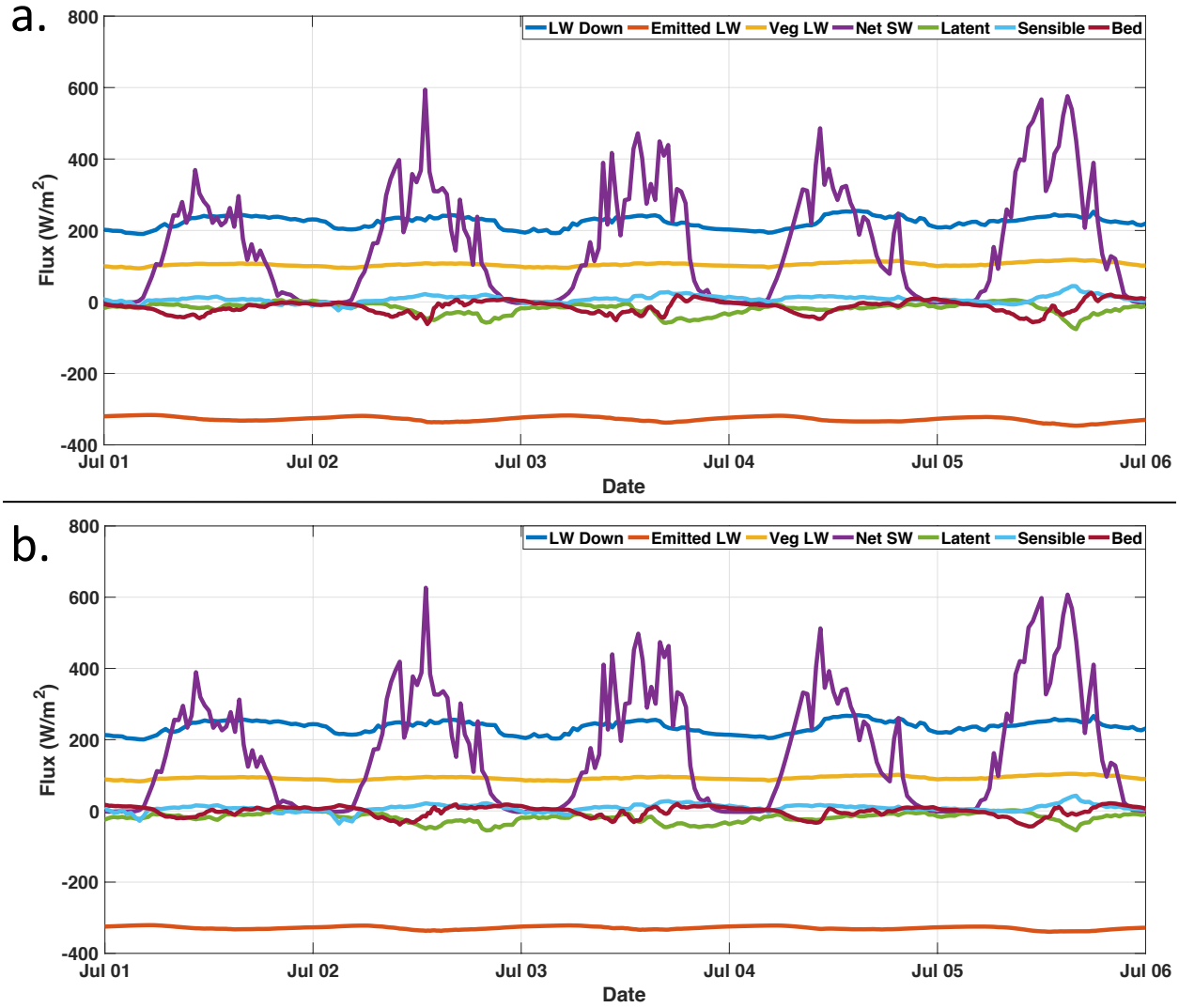

Figure 3.21 Distributed energy fluxes averaged over the study reaches (1950 m) for July 1 to 6, 2016 in GC (a) and BB (b). LW Down is incoming longwave radiation, Emitted LW is longwave radiation emitted by the stream surface, Veg LW is longwave radiation emitted by vegetation, Net SW is net shortwave radiation, Latent is the latent heat flux, Sensible is the sensible heat flux, and Bed is the bed conductive heat flux.

Tables

Table 3.1 Summary of distributed energy fluxes over the study period (June 22 to September 5, 2016) for GC and BB.

	Mean Daily Distributed Energy Fluxes (MJ/m^2Day)	
Variable	**Granger Creek**	**Buckbrush Creek**
Net Shortwave Radiation	9.79	10.32
Net Longwave Radiation	0.42	0.34
Latent Heat	-1.27	-1.38
Sensible Heat	0.19	0.19
Bed Conduction	-1.14	-0.02
Net	7.99	9.45